University Paul Sabatier

Un joli titre

Flaurent HEULLY–ALARY

September 5, 2025

Contents

Chapter 1

Introduction

Chapter 2

Theory and Methodology

2.1 Model Hamiltonian

2.1.1 Spin Hamiltonian

Heiseinberg Hamiltonian

The most well-know Spin Hamiltonian used to describe the magnetic interaction between a pair of spin located on different magnetic centres is the Heiseinberg-Dirac-Van Vleck (HDVV) Hamiltonina, written as:

$$\hat{H}_{HDVV} = -\sum_{i,j} J_{ij} \hat{\mathbf{S}}_i \cdot \hat{\mathbf{S}}_j \tag{2.1.1}$$

where $J_{i,j}$ is the coupling constant, $\hat{\mathbf{S}}_i$ and $\hat{\mathbf{S}}_j$ are the spin operators working on site i and j. Several conventions exist for this Hamiltonian, with negative sign and/or a factor of 2 in front. The coupling constant J can be either positive or negative depending on the magnetic properties of the system, a positive value indicate ferromagnetism with magnetic moment aligned while negative indicate antiferromagnetism with opposite alignement of magnetic moments. This Hamiltonian is regarded as a Spin Hamiltonian as it only invoke the spin degree of freedom of the system and is still to this day used in the description of the isotropic coupling in magnetic systems.

The J constant is defined as an effective integral as it involves several mechanisms:

1- Direct exchange originating from the exchange integral K.

2- Indirect exchange involving ionic determinants.

3- Super-exchange where a diamagnetic bridging ligand open new pathway for exchange mechanisms.

The origins and contributions of these mechanisms to the effective integral can be understood from the Hubbard Hamiltonian in the case of two electrons in two orbitals. Up to the second order perturbation theory, the following expression can be obtained for the effective integral J:

$$J = 2K - \frac{4t^2}{U} \tag{2.1.2}$$

Where K is the exchange integral which is always positive, t the hopping integral between the two orbitals and U the on site Coulomb repulsion. This expression shows the competition between a ferromagnetic component (direct exchange $K>0$) and an antiferromagnetic one (indirect exchange). The contribution of super-exchange cannot be estimated at second-order and requires going up to fourth-order pertubation giving a similar expression:

$$J = 2K - \frac{4t_{eff}^2}{U} \tag{2.1.3}$$

Where t_{eff} is now an effective hopping integral involving the bridging ligand, the hopping term between metallic to ligand being much larger than the metallic to metallic one, the t term is usually neglected in this expression. Note that the perturbation expansion is valid only in case of $U >> t$, when the system's behavior is not dominated by delocalisation that would render the HDVV Hamiltonian inadecate.

Ising Hamiltonian

The eigenfunctions of the Heiseinberg Hamiltonian are eigenfunctions of the $\hat{\mathbf{S}}^2$ operator, making them mostly multi-determinental functions which can only be obtained via specific computational methods. To draw an easier picture, it is possible to restrict the spin vector to its component along the z axis alone.

$$H_{ising} = -\sum_{i,j} J_{ij} \hat{\mathbf{S}}_{z,i} \hat{\mathbf{S}}_{z,j} \tag{2.1.4}$$

The magnetic moment of each lattice site are now considered to align themselves with the z axis at all time, taking a ± 1 value. The main advantage of this approximation is that the eigenfunctions of this Hamiltonian are now mono-determinantal functions opening up the extraction to new computation methods. It also reduces the analytical derivation allowing to work on larger systems without the need to diagonaize large matrices.

2.1.2 Mononuclear Anisotropy

Effects such as Spin-Orbit-Coupling (SOC) tend to create anisotropy in the system that cannot be described only by eq (2.1.1). More specifically on mononuclear systems (only one magnetic centre) with a ground state of spin larger or equal to one and correct symmetry conditions, a lift of degeneracy between the different M_S component of a same S state can be observed even in the absence of magnetic field, this phenomenon is called Zero-Field-Splitting. The associated Spin Hamiltonian is written:

$$\hat{H}_{ZFS} = \hat{\mathbf{S}} \cdot \overline{\overline{D}} \cdot \hat{\mathbf{S}} \tag{2.1.5}$$

Where $\hat{\mathbf{S}}$ is the spin vector of the ground state and $\overline{\overline{D}}$ is a two rank symmetric tensor, in an arbitrary frame it is composed of six different parameters.

$$\overline{\overline{D}} = \begin{pmatrix} D_{xx} & D_{xy} & D_{xz} \\ D_{xy} & D_{yy} & D_{yz} \\ D_{xz} & D_{yz} & D_{zz} \end{pmatrix} \tag{2.1.6}$$

This tensor can be reduced to three parameters by diagonalization, *i.e* expressing them in the the tensor principal axes that define the magnetic anisotropy axes. Going further as to work with traceless tensor allow us to use only two parameters, by convention the z-axis is taken as the main magnetic axis with D the axial parameter:

$$D = D_{zz} - \frac{1}{2}(D_{xx} + D_{yy}) = \frac{3}{2}D_{zz} \tag{2.1.7}$$

and the rhombic term:

$$E = \frac{1}{2}(D_{xx} - D_{yy}) \tag{2.1.8}$$

With $|D| \geq 3E \geq 0$. The ZFS Hamiltonian can then be written:

$$\hat{H}_{ZFS} = D(\hat{S}_z^2 - \frac{1}{3}\hat{S}^2) + E(\hat{S}_x^2 - \hat{S}_y^2) \tag{2.1.9}$$

A positive value of D indicates that the ground state is mainly composed of the M_S=0 component meaning that the projection of the spin moment along the z-axis is close to zero resulting in a easy-plane magnetism. On the contrary if D<0, the ground state is formed from the M_S=$\pm M_{Smax}$ components with a maximum projection of spin moment along the z-axis resulting in an easy-axis magnetism. For a ground state with spin larger than one and a half, other terms may appear but will not be reported in this work. (Rajouter le B40)

In the case of a triplet S=1 ground stat such as a nickel Ni (II) complex, the matrix representation of hamiltonian (2.1.5) in a random set of axis:

H_{ZFS}	$\|1,-1\rangle$	$\|1,0\rangle$	$\|1,1\rangle$
$\langle 1,-1\|$	$\frac{1}{2}(D_{xx} - D_{yy}) + D_{zz}$	$-\frac{\sqrt{2}}{2}(D_{xz+iD_{yz}})$	$\frac{1}{2}(D_{xx} - D_{yy} + 2iD_{xy})$
$\langle 1,0\|$	$-\frac{\sqrt{2}}{2}(D_{xz-iD_{yz}})$	$D_{xx} + D_{yy}$	$\frac{\sqrt{2}}{2}(D_{xz} + iD_{yz})$
$\langle 1,1\|$	$\frac{1}{2}(D_{xx} - D_{yy} - 2iD_{xy})$	$\frac{\sqrt{2}}{2}(D_{xz} - iD_{yz})$	$\frac{1}{2}(D_{xx} + D_{yy}) + D_{zz}$

In the magnetic frame, this matrix becomes:

H_{ZFS}	$\|1,-1\rangle$	$\|1,0\rangle$	$\|1,1\rangle$
$\langle 1,-1\|$	$\frac{1}{2}(D_{XX} + D_{YY}) + D_{ZZ}$	0	$\frac{1}{2}(D_{XX} - D_{YY})$
$\langle 1,0\|$	0	$D_{XX} + D_{YY}$	0
$\langle 1,1\|$	$\frac{1}{2}(D_{XX} - D_{YY})$	0	$\frac{1}{2}(D_{XX} + D_{YY}) + D_{ZZ}$

Removing the trace from the tensor and applying the convention from eq(2.1.7) and eq(2.1.8) we get:

H_{ZFS}	$\|1,-1\rangle$	$\|1,0\rangle$	$\|1,1\rangle$
$\langle 1,-1\|$	$\frac{1}{3}D$	0	E
$\langle 1,0\|$	0	$\frac{2}{3}D$	0
$\langle 1,1\|$	E	0	$\frac{1}{3}D$

Note that in the case of an even number of unpaired electron, the D and E parameter can be estimated directly from the energy spectrum. In the case of a triplet ground

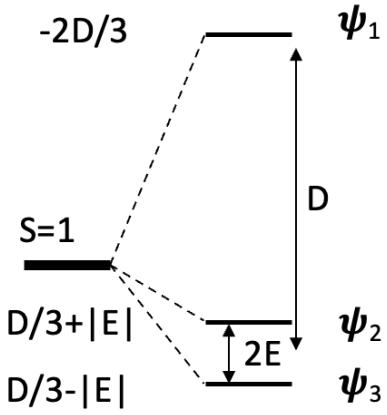

Figure 2.1: Schematic representation of the three lowest SO-state undergoing ZFS in the case of triplet ground state.

state, diagonalizing the model Hamiltonian matrix gives the three eigenvalues:

$$E_1 = -\frac{2}{3}D \tag{2.1.10}$$

$$E_2 = \frac{1}{3}D + E \tag{2.1.11}$$

$$E_3 = \frac{1}{3}D - E \tag{2.1.12}$$

with the eigenvectors:

$$\psi_1 = |1,0\rangle \tag{2.1.13}$$

$$\psi_2 = \frac{1}{\sqrt{2}}(|1,-1\rangle + |1,1\rangle) \tag{2.1.14}$$

$$\psi_3 = \frac{1}{\sqrt{2}}(|1,-1\rangle - |1,1\rangle) \tag{2.1.15}$$

leading to the extraction of the D and E terms directly from the energies:

$$D = \frac{1}{2}(E_2 + E_3) - E_1 \tag{2.1.16}$$

and

$$E = \frac{1}{2}(E_2 - E_3) \tag{2.1.17}$$

2.1.3 Polynuclear Anisotropy

Opening the study to multiple magnetic center introduces weak couplings between the magnetic moments of each center. This coupling between two sites A and B with at

lest one magnetic electron each, is called exchange interaction and is described by the following Giant Spin Hamiltonian.

$$\hat{H}_{AB} = \hat{\mathbf{S}}_A \cdot \overline{\overline{D}} \cdot \hat{\mathbf{S}}_B \tag{2.1.18}$$

The spin-spin interaction tensor $\overline{\overline{D}}$ describes Zero-Field-Splitting the same way as before but now between two sites A and B, two parameters D and E can be defined similarly. This Hamiltonian is suitable for system with a ground state of spin larger or equal to one that is well separated in energy from other SO-states. It is also possible to study cases where mixing with low-lying excited states occurs by decomposing the tensor $\overline{\overline{D}}$ in three terms.

$$\hat{H}_{AB} = J(\hat{\mathbf{S}}_A \cdot \hat{\mathbf{S}}_B) + \hat{\mathbf{S}}_A \cdot \overline{\overline{D}}_{AB} \cdot \hat{\mathbf{S}}_B + \mathbf{d}_{AB} \cdot (\hat{\mathbf{S}}_A \times \hat{\mathbf{S}}_B) \tag{2.1.19}$$

Where the first term is the isotropic exchange, extending this coupling to more than two center this term becomes equivalent to the HDVV Hamiltonian from (2.1.1). The two following terms describe the anisotropic exchange with the symmetric tensor of exchange $\overline{\overline{D}}_{AB}$ and the antisymmetric exchange $\mathbf{d}_{AB}$ also called Dzyaloshinskii-Moriya pseudo-vector interaction. For couplings involving more than one unpaired electron per site, local tensor are introduced:

$$\hat{H}_{AB} = J(\hat{\mathbf{S}}_A \cdot \hat{\mathbf{S}}_B) + \hat{\mathbf{S}}_A \cdot \overline{\overline{D}}_{AB} \cdot \hat{\mathbf{S}}_B + \mathbf{d}_{AB} \cdot (\hat{\mathbf{S}}_A \times \hat{\mathbf{S}}_B) + \hat{\mathbf{S}}_A \cdot \overline{\overline{D}}_A \cdot \hat{\mathbf{S}}_A + \hat{\mathbf{S}}_B \cdot \overline{\overline{D}}_B \cdot \hat{\mathbf{S}}_B \tag{2.1.20}$$

The matrix representation for two spin $1/2$ systems interacting is the following:

H_{MS}	$\lvert 1,-1\rangle$	$\lvert 1,0\rangle$	$\lvert 1,1\rangle$	$\lvert 0,0\rangle$
$\langle 1,-1\rvert$	$\frac{J}{4} + \frac{D_{zz}}{4}$	$\frac{D_{xz}-iD_{yz}}{2\sqrt{2}}$	$\frac{(D_{xx}-D_{zz}-2iD_{xy})}{4}$	$\frac{d_y+id_x}{2\sqrt{2}}$
$\langle 1,0\rvert$	$\frac{D_{xz}+iD_{yz}}{2\sqrt{2}}$	$\frac{J}{4} - \frac{D_{zz}}{4} + \frac{(D_{xx}+D_{yy})}{4}$	$-\frac{D_{xz}-iD_{yz}}{2\sqrt{2}}$	$-\frac{id_z}{2}$
$\langle 1,1\rvert$	$\frac{(D_{xx}-D_{zz}+2iD_{xy})}{4}$	$-\frac{D_{xz}+iD_{yz}}{2\sqrt{2}}$	$\frac{J}{4} + \frac{D_{zz}}{4}$	$\frac{d_y-id_x}{2\sqrt{2}}$
$\langle 0,0\rvert$	$\frac{d_y-id_x}{2\sqrt{2}}$	$\frac{id_z}{2}$	$\frac{d_y+id_x}{2\sqrt{2}}$	$-\frac{3J}{4} - \frac{D_{zz}}{4} - \frac{(D_{xx}+D_{yy})}{4}$

From this matrix we notice that the Dzyaloshinskii-Moriya interaction create a coupling between the singlet with the three M_S components of the triplet state. As for the symmetric tensor of anisotropic exchange, it only couples the three component of the triplet which undergo a splitting in energy. At the isotropic level, the difference between the triplet and singlet state is given by $\Delta E = J$, but with the inclusion of the anisotropic terms this becomes much more complex. As opposed to the Zero-Field Splitting mechanism, it is impossible to obtain values for these interactions from the energy spectrum only, as such they will be extraced from effective Hamiltonian theory. Note that now the application of this Hamiltonian is not restricted to a ground state with $S \geq 1$ but can be used for a singlet or doublet case. All of these considerations are only possible in the strong exchange limit where the isotropic coupling is large compared to the anisotropic interactions.

2.2 Methodology

All types of calculations discussed here after have for purpose to solve, in some way, the Schrodinger Equation:

$$\hat{H}\Psi_i = E_i\Psi_i \tag{2.2.1}$$

Where $\hat{H}$ is an Hamiltonian used to describe the system studied, E_i is the energy associated to the wave-function Ψ_i. The solutions E_i of this problem are obtained pretty straightforwardly by diagonalizing the Hamiltonian except that in most cases, the Ψ_i vector are not known beforehand. The Hamiltonian treated during the calculations is called exact electronic Hamiltonian as it encapsulate all the electronic and nuclear interaction of the system, it is written as follow in atomic units:

$$\hat{H} = -\sum_{i=1}^{N}\nabla_i^2 - \sum_{A=1}^{M}\frac{1}{2M_A}\nabla_A^2 - \sum_{i=1}^{N}\sum_{A=1}^{M}\frac{Z_A}{|r_i - R_A|} + \sum_{i=1}^{N}\sum_{j<i}^{N}\frac{1}{r_{ij}} + \sum_{A=1}^{M}\sum_{B>A}^{M}\frac{Z_A Z_B}{|R_A - R_B|} \tag{2.2.2}$$

Where r_i is the position vector of the ith electron, R_A the position vector of the Ath nucleus with atomic number Z_A and mass M_A. This Hamiltonian can be simplified in the context of the Born-Oppenheimer approximation, the electrons are considred to adapt instantly to the movement of the nuclei, the latter's position can be fixed and taken out of the Hamiltonian. This approximation is justified with the fact that the electrons are much lighter than the nuclei.

$$\hat{H}_{elec} = -\frac{1}{2}\sum_{i=1}^{N}\nabla_i^2 - \sum_{i=1}^{N}\sum_{A=1}^{M}\frac{Z_A}{|r_i - R_A|} + \sum_{i=1}^{N}\sum_{j<i}^{N}\frac{1}{|r_i - r_j|} \tag{2.2.3}$$

This Hamiltonian describes the electronic problem while the nuclei contribution is set aside in a constant, having for only effect a shift in the overall energy spectrum. While this greatly simplify the equations, it is still not solvable analyticaly and several approximations were developped to tackle this problem. One common point to all the methods that were used in this work rely on the construction of molecular orbitals (**MO**) as expansions of atomic orbitals (**AO**).

$$\psi_k = \sum_i c_i\phi_i \tag{2.2.4}$$

Where ψ_k is the kth MO built from the AO ϕ_i with the coefficient c_i. This expansion rely on a supposedly infinite number of AO but in real case application this is not achievable and will thus be restricted to a finite number of basis functions. As the eletronic Hamiltonian does not include any information about spin, it will be included within a so called spin orbital with the introduction of two orthonormal function $\alpha(\omega)$ and $\beta(\omega)$, *i.e* spin up or down function, with ω an unspecified spin variable. From each

spatial molecular orbital, two spin orbital can be created such that:

$$\chi_i = \begin{cases} \psi_i(r)\alpha(\omega) \\ \quad or \\ \psi_i(r)\beta(\omega) \end{cases} \tag{2.2.5}$$

This definition for the spin orbital is well adapted for closed shell systems where all molecular orbitals are doubly occupied, the spatial part for any spin orbital is the same for both spin function defining the restricted formalism. Such definition changes when working with open shell system, *i.e* some orbitals are singly occupied necessiting the application of unrestricted formalism.

2.2.1 Hartree-Fock Method

The cornersone of *ab initio* calculation in quantum chemistry is the Hartree-Fock method which is usually the initial step for computing a first approximation of the wave function in molecules. It is a variational approach that aims to treat the N-electron problems as problem of N non interacting electrons in the presence of an average potential replicating interactions between them, it is in this sense a mean-filed theory. This wave-function is constructed on the optimisation of a single Slater determinant Ψ:

$$\Psi(x_1, x_2, \ldots, x_N) = \frac{1}{\sqrt{N!}} \begin{vmatrix} \chi_i(x_1) & \chi_j(x_1) & \cdots & \chi_k(x_1) \\ \chi_i(x_2) & \chi_j(x_2) & \cdots & \chi_k(x_2) \\ \vdots & \vdots & & \vdots \\ \chi_i(x_N) & \chi_j(x_N) & \cdots & \chi_k(x_N) \end{vmatrix} \tag{2.2.6}$$

Where χ_i are spin orbitals and the variable $x_i = \{r_i, \omega_i\}$, it involves all combination of all N electrons in all k spin orbitals. We introduce the shorthand notation for such determinant $\Psi(x_1, x_2, \ldots, x_N) = |\chi_1\chi_2 \ldots \chi_k\rangle$ showing only the diagonal elements of the determinant.

The way to obtain the best adapted Hartree-Fock wave function comes through the resolution of the Roothan's equation:

$$FC = SC\epsilon \tag{2.2.7}$$

S is the overlap matrix of the basis function, ϵ the matrix of orbital energies and C is the matrix of the trial vector. The Fock operator F is defined as:

$$\hat{F}(i) = \hat{h}(i) + \sum_{j}^{N/2} [2\hat{J}_j(i) - \hat{K}_j(i)] \tag{2.2.8}$$

The core-Hamiltonian $\hat{h}(i)$ is a mono-electronic operator that contains the kinetic energy operator of the ith and coulomb repulsion with the fixed nuclei. The two bieletronic operator $\hat{J}_j(i)$ and $\hat{K}_j(i)$ describe the coulomb repulsion and exchange mechanism between the ith electron and the rest. These operator carry a direct dependance on the trial vectors from eq 2.2.7 as such, the Roothan's equation are non-linear and will be solved iteratively following a *Self Consistent Field* (SCF) procedure.

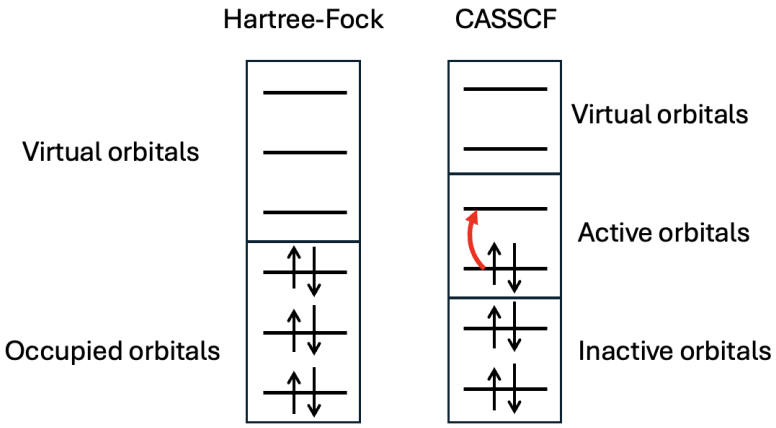

Figure 2.2: Difference between the orbitals space in Hartree-Fock and CASSCF Theory

2.2.2 Complete Active Space Self Consistent Field

For most of magnetic systems, a single reference wave function is not enough as the system is usually not closed-shell and present one or more unpaired electron. Hence, its ground state is described by a wave function composed of several determinants. One of the most used method to introduce multiple reference in the wave function is called *Complete Active Space Self Consistent Field* (*CASSCF*). Compared to the Hartree-Fock theory where two types of orbitals (occupied and unoccupied) were considered, in CASSCF theory orbitals are separeted in three sub-space. The inactive orbitals are doubly occupied throughout the calculation, virtual orbitals will stay empty while the active orbitals have a variable occupancy ranging from zero to two electrons. These active orbitals define the active space into which a configuration interaction will be realised computing all the determinants possible within this sub-space. As the number of determinant grows significally with the number of orbitals included in the active space, this method is quite costly and its size becomes a limiting factor for the calculations. The new wave functions is now written as an expansion of Slater determinant which is obtained via a SCF procedure where both the expansion coefficients and orbitals are optimised as to minimize the Schrodinger Equation. This double optimisation scheme can render the convergence troublesome, as such the definition of the active space and the choice of the starting orbitals becomes crucial. One usually starts from a set of orbitals previously obtained via an Hartree-Fock calculation. For computation of magnetic properties in transition metal systems, the minimum active space should consists of the magnetic orbitals, *i.e* the singly occupied d-orbitals of the metalic centers, this can later be extended to all of the 3-d orbitals of the metal as well as some orbitals of the ligands. As a result of the CASSCF method we obtain the energies of all states included in the calculation and a new set of orbitals into which they are expressed. This calculation takes into account the correlation between the

electrons inside the active space in the mean field created by the other electrons. While this method provides the non-dynamical correlation, it fails to capture the correlation with the inactive electron and their reponse to excitations, called dynamic-correlation and the need to look further appears.

2.2.3 Perturbation Theory

Perturbative treatment can be applied to extract the dynamical correlation of the mono and diexcitations that is left out from simple CASSCF calculation. For such calculation, one can use the CASPT (Complete Active Space Perturbation theory) or the NEVPT (N-electron valence state perturbation theory). Both of these methods rely on the assumption that the Hamiltonian can be partitioned into a zeroth order term and a perturbation with the parameter λ:

$$\hat{H} = \hat{H}^{(0)} + \lambda\hat{H}^{(1)} + \lambda^2\hat{H}^{(2)} + \dots \tag{2.2.9}$$

The wave function and energy are expanded in a similar way and the zeroth order term $\Psi^0_{(0)}$ is chosen to be the CASSCF wave function. The effect of the configurations outside of the active space on the energy and the wave function is estimated though perturbation theory and the expansions of the equations allows one to obtain the corrected energies usually at second order of perturbation with CASPT2 or NEVPT2. These two method mainly differs from their chose of zeroth-order Hamiltonian, CASPT2 rely on a monoelectronic Hamiltonian built from a one electron Fock operator that falls back to the Moller-Plesset Hamiltonian in single reference case. This treatment may lead to what is called "intruder states" where low-lying states induce divergence in the denominator of the correction term where a difference of energy is taken. Several approach have been adapted such a the introduction of a *level shift*, real or imaginary, as to fix this divergence. In case of NEVPT2, the zeroth-order Hamiltonian is a bi-electronic Dyall Hamiltoninan which in itself include a shift in energy between state from inside or outside the active space preventing the appearance of intruder states. One should add that this correlation is considered contracted as these methods do not act upon the coefficients inside the wave functions but only on the energies.

2.2.4 Difference dedicated configurational interaction

To get a full picture of the dynamic correlation one has to go to Multi-Referential-Configuration-Interaction (MRCI) methods. This method allows to introduce new determinants in the wave-function that do not belong to the CASSCF space, this way not only the energies but the wavefunction itself is revised. While very promising this method is not applicable to any real systems because of the number of determinants to include in the CI expansion, the cost of calculation becoming too high one has to truncate the MRCI space. Restricting the CI to all the simple and double excitations is still not feasible as they are too numerous, but some of them can be left out of the calculations. These excitations are classified into eight categories depending on the number of hole/particle created represented on figure 2.3. A hole is an excitation from

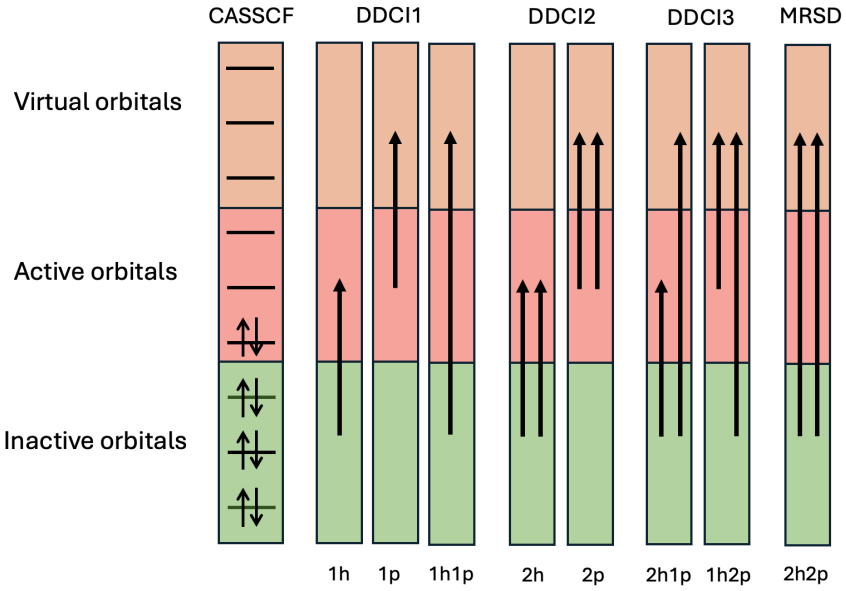

Figure 2.3: Classes of excitations and associated DDCI method

a inactive orbital to an active or virtual orbital, while a particle is an excitation from an active or inactive orbital to a virtual one.

The most troublesome excitations are the one generating two holes and two particles (2h-2p) as they are the most numerous, but it can be shown at second order of perturbation that they do not contribute to the energy difference but only act as a shift of the diagonal energies. As such they can be neglected giving rise to a variant of MRCI called Difference-Dedicated-Configurational-Interaction (DDCI). Three sub-variant of DDCI exists taking into account differents classes of excitations as pictured on fig 2.3 It has been established that the extraction of magnetic coupling involving bridging ligand requires the use of the DDCI3 method to provide good estimates.

2.2.5 Density functional theory

Another way to get a description of the electronic structure of is through density functional theory (DFT). The main interest of such method is the description of the ground state properties through the determination of the ground state energy E_0 following the variationl theorem:

$$E_0 = \min \langle \Psi | \hat{H} | \Psi \rangle \tag{2.2.10}$$

Here, the eletronic wavefunction of the molcule Ψ is approximated to a single Slater determinant obtained from the determination of the electronic density $\rho(\mathbf{r})$:

$$\rho(\mathbf{r}) = N \int |\Psi(\mathbf{x}_1 \dots \mathbf{x}_N)|^2 ds_1 dx_2 \dots dx_N \tag{2.2.11}$$

The Hamiltonian2.2.3 can be written:

$$\hat{H} = \hat{T} + \hat{V}_{ee} + \hat{V}_{ne} \tag{2.2.12}$$

with $\hat{T}$ the kinetic energy operator, $\hat{V}_{ee}$ the electron-electron interaction operator and $\hat{V}_{ne}$ the nuclei-electron interaction operator. By replacing $v_{ne}(\rho\mathbf{r})$ with a known external potential $v(\mathbf{r})$, one can obtain the ground state wave function Ψ by solving the Shrodinger equation giving the electron density follows. The first Hohenberg-Kohn theorem states that this external potential is an unique functional of the electron density. As such, knowing the electron density allows to determine the properties of the ground states. The second Hohenberg-Kohn gives in case of non degenerate ground state, the wave function Ψ is itself a functionl of $\rho(\mathbf{r})$ which allow to define the total energy:

$$E[\rho] = F[\rho] + \int \rho(\mathbf{r})v(\mathbf{r})dr \tag{2.2.13}$$

with $F[\rho]$ an universal density functional which contain the kinetic and potential contributions. The ground state energy E_0 is the minimum of eq 2.2.13 which is reached when the electron density is that of the gound state $\rho_0(\mathbf{r})$. In theory the knowledge of the electon densty allows to determine E_0, however the density dependance expression of $F[\rho]$ is not known.

$$F[\rho] = T[\rho] + V_{ee}[\rho] \tag{2.2.14}$$

Kohn and Sham introduced new definition of this functional by replacing the interacting system with a fictious system of N non interacting electronsThe functional becomes:

$$F[\rho] = T_s[\rho] + J[\rho] + E_{xc}[\rho] \tag{2.2.15}$$

Where $T_s[\rho]$ is the non interacting kinetic energy functional of density ρ expressed in the basis of $\phi_i(\mathbf{r})$ that are built to reproduce the ground state density $\rho(\mathbf{r})$.

$$\rho(\mathbf{r}) = \sum_i^N |\phi_i(\mathbf{r})|^2 \tag{2.2.16}$$

$$T_s[\rho] = \sum_i^n \langle\phi_i| - \frac{1}{2}\nabla^2 |\phi_i\rangle \tag{2.2.17}$$

The Hartree-potential $J[\rho]$ gives the coulomb repulstion between electrons pair:

$$J[\rho] = \frac{1}{2}\int\int \frac{\rho(\mathbf{r}_1)\rho(\mathbf{r}_2)}{|\mathbf{r}_2 - \mathbf{r}_1|} d\mathbf{r}_1 d\mathbf{r}_2 \tag{2.2.18}$$

The energy expression eq 2.2.13 finally becomes:

$$E[\rho] = \int v(\mathbf{r})\rho(\mathbf{r})d\mathbf{r} + T_s[\rho] + J[\rho] + E_{xc}[\rho] \tag{2.2.19}$$

This definition gives the exact energy given that the expression of the Exchange-Correlation E_{xc} is known, unfortunately this is not the case. Over the years multiple

attempts have been made to find an universal expression of E_{xc} in terms of ρ and its derivative. In the most basic approach, called Local Density Approximation (LDA), the system is taken to behave as a uniform electron gas where E_{xc} depends only in the density ρ. This model was later adapted to study different spin configuration with the Local Spin Density Approximation (LSDA). Other attemps tried to improve the functional by incorporating a dependance in the derivative of ρ with the Generalized Gradient Approximation (GGA) or a small portion of the Hartree-Fock exact exchange in what is called hybrid functionals.

2.2.6 Embedded Cluster Method

In the case of molecules, the study of magnetic anisotropy is well described by single molecule calculations as these interactions are localised between the metallic centers and ligands. The restricted size of the molecule generally allows for an explicit treatment of all the atoms involved. The same cannot be said about cristalline systems which are considred infinite but cannot be treated that way by the methods chosen in this work, as such we have to work on smaller part called "cluster" or "fragment". In theory one would want the fragment to be as large as possible to reduce the error created by cutting off the fragment of its environment, unfortunately to reduce computational cost we have to limit ourselves with small sized fragments. It then becomes crucial to chose correctly the fragment based on our knowledge of the physics we want to include. The properties of the cluster alone differ from the one inside its natural environment, to reproduce them accurately it is immersed inside an embedding. This embedding is composed of point charges that aim to replicate the electrostatic field of the crystal inside the cluster region, called Madelung Field. To keep the symmetries of the crystal, the point charges are positionned at the lattice site in a sphere of radius R_c. Another problem in

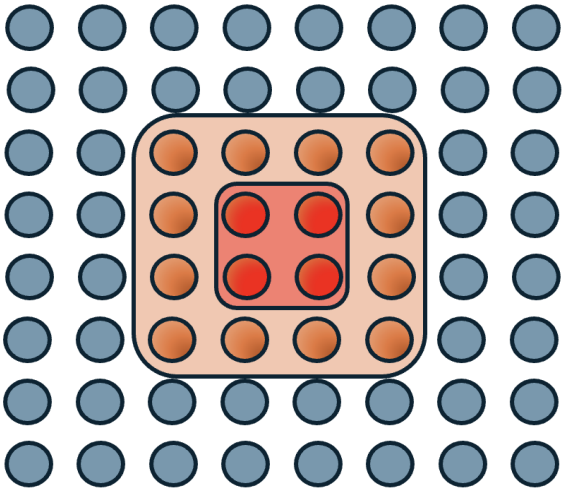

Figure 2.4: Schematic representation of the three region composing the embedding. red: cluster, orange: TIPS, blue: point charges

selecting fragments in ionic crystal is the overall charge of the fragment. The centre of

the study is the metallic ions, charged positively, forming ionic bonds with negatively charged ligand. A correct description of these magnetic centre requires to include all closest neighbors which makes the overall fragment negatively charged. The ions at the border of the fragment, replaced by point charges, are then positive. This induces a polarization of the electron density of the anions bordering the cluster. To avoid the electrons escaping the fragment, pseudo-potentials are placed at the lattice sites near the fragment to act as walls which prevent electrons from approaching these positive charges as if they were real atoms. These potentials are called Total-Ion-Potentials (TIPS) and can be either *ab initio* model potential (AIMP) or Effective Core Potential (ECP) depending on which Quantum Chemistry software is used.

Two procedure were explored to create such embedding:

(1) Formal charges were used in a sphere with very large R_c (around 50 Å).

(2) Optimised point charges were obtained using Ewal Summation from formal charges, this allows to reduce the R_c to a few angstrom around the fragment.

All of this is done to ensure that the properties extracted from the fragment, *i.e* a finite system, are a good representation of the crystal properties, *i.e* an infinite system.

2.2.7 Effective Hamiltonian

Having ways to compute the *ab initio* multi reference wave functions usually leads to lenghty expression where the wave function is spanned along a large number of Slater determinant making its analysis complicated. On the other hand, the model Hamiltonian work in a much smaller space where a small number of electrons is used to introduce effective interactions. A way to connect the two Hamiltonians is to apply a theory developped by Bloch called Effective Hamiltonian theory. Its purpose is to build an effective Hamiltonian whose eigenvalues reproduce the energy spectrum of the *ab initio* Hamiltonian but using a much smaller number of eigenfunctions.

Starting from the Schrodinger equation with the Born-Oppenheimer Hamiltonian $\hat{H}$:

$$\hat{H} \left|\Psi_m\right\rangle = E_m \left|\Psi_m\right\rangle \tag{2.2.20}$$

Where Ψ_m are the eigenvectors with the associated eigenvalue E_m forming the space S of size N. We define a smaller space S_0 with N_0 states, this space is usually composed of the low lying state where the model Hamiltonian will be developped. An effective Hamiltonian H_{eff} is built to reproduce the energy spectrum of the exact Hamiltonian in the target space S_T using a small number of low-lying states $\tilde{\Psi}_m$ such that:

$$\hat{H}_{eff} \left|\tilde{\Psi}_m\right\rangle = E_m \left|\tilde{\Psi}_m\right\rangle \tag{2.2.21}$$

This target space S_T is chosen to be the same as the model space S_0 allowing for direct comparison. The first step is to project the eigenfunctions Ψ_m onto the model space using the projector:

$$\hat{P}_0 = \sum_m^{N_0} |\tilde{\Psi}_m\rangle \langle\tilde{\Psi}_m| \tag{2.2.22}$$

$$|\tilde{\Psi}_m\rangle = \hat{P}_0 |\Psi_m\rangle \tag{2.2.23}$$

These eigenvectors are not necesserily orthogonal leading to a non-Hermitian Hamiltonian, this is problematic when comparing to the model Hamiltonians which are Hermitians. In this work, we apply the formalism proposed by Des Cloizeaux where the vectors are symmetrically orthonalized from the overlap matrix S:

$$|\tilde{\Psi}_m^{\perp}\rangle = S^{-1/2} |\tilde{\Psi}_m\rangle \tag{2.2.24}$$

At this point, it is possible to check the quality of the target space by calculating the norm of the projected vectors present in the S matrix. If too small, the interactions of the system are not captured correctely by the model space making it inadecate.

When these projections are close to one, we can consider the model space adecate, the effective Hamiltonian is then built:

$$H_{eff} = \sum_m^{N} |\tilde{\Psi}_m^{\perp}\rangle E_m \langle\tilde{\Psi}_m^{\perp}| \tag{2.2.25}$$

Once this is done, this numerical matrix H_{eff} constructed from the *ab initio* exact Hamiltonian are compared to the model Hamiltonian representation matrix. This allows for the extraction of values for the model Hamiltonian parameters as well as a test of validity. If there is too much deviation between the two matrices, it is possible that there is some missing interaction in the model.

Chapter 3

Study of the anisotropy in mononuclear complexes

The field of mononuclear complexes is a perfect area for the study of magnetic anisotropy. The finite size of such complex as well as the localised character of the interaction allow for the explicit treatment of all atoms at play with reasonnable computational cost. This combined with the large amount of experimental data available allow for the validation of models and computational methodology. Numerous studies were dedicated to the application of the ZFS model Hamiltonian on mononuclear complexes based on fourth period transition metal. It has established that the value of the ZFS parameters are highly dependant on the metallic ion and its environment, the choice of ligand is crucial as we will see in this chapter.

State of the art methodology for such study is to generate a wavefunction from a CASSCF calcuation including all electronic state generated by an active space composed of all the d orbitals of the metallic ion and the electrons occupying them. Dynamic correlation is taken into account by pertubation with NEVPT2 including all the states from the CASSCF calculation. Spin orbit coupling between M_S component of all states are accounted for using Spin-Orbit-State-Interaction with NEVPT2 correlated energies as the diagonal of the SO matrix. Finally, ZFS parameters are extracted following the Effective Hamiltonian Theory in a procedure implemented in the ORCA package.

3.1 First Order Spin Orbit Coupling

The ideal case for creating large anisotropy is to approach first order spin orbit coupling regime. First order spin orbit coupling arises when a two-fold degenerate ground state is formed from configuration with degenerate d-orbitals as represented on figure 3.1 in case of d^6 configuration in D_{5h} geometry.

These two states would be strongly coupled via 1^{st}order SOC resulting in a large splitting of the M_S component of the ground state with a large value for the D term as strong as the spin orbit coupling constant. In reality a lift of degeneracy of the d orbitals is induced from the coordination sphere stabilising one of the two configurations, making it the main component of the ground state, and destabilising the other to an

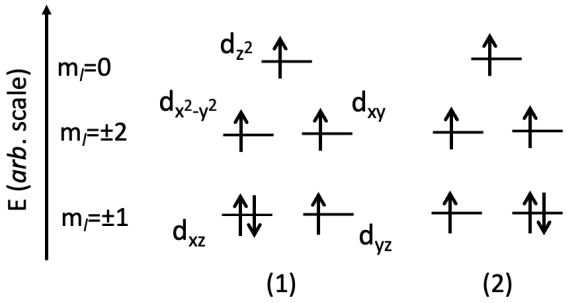

Figure 3.1: The two degenerate configurations for d^6 configuration in ideal D_{5h} geometry

excited state. This loss of symmetry greatly reduces energy splitting of M_S component and may induce rhombicity in the system. At this stage the angular momentum L is quenched making the spin momentum S a "not-too-bad" quantum number, allowing the application of the ZFS model Hamiltonian formalism with the extraction of a D axial parameter and rhombic terme E. The remaining anisotropy is the result of second order spin orbit coupling from the ground state with low-lying exicted states. This interaction stems from the excitation of an electron from a d orbital to a higher-energy orbital as depicted on figure **??** and its magnitude rely on the difference in energy between the orbitals. Small energy differences (a few hundred cm^{-1}) between the orbital allow to retrieve a contribution of 1^{st}order SOC increasing the value of D. It has then become an interest to find ligands that satisfy this condition of quasi-degeneracy of the d-orbital.

With this in mind, a series of five Iron(II) complexes were synthesized in a heptacoordinated environment with different apical ligands (X and Y positions in figure 3.2).

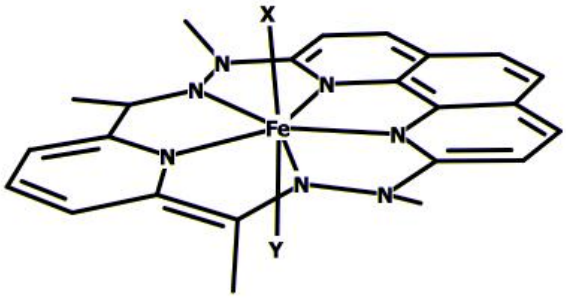

Figure 3.2: Schematic representation of the complex with H atoms attached to carbon hidden

3.2 Impact of the Electric field on the ZFS parameters

This chapter is the follow up of a previous study on a Nickel II complex exhibiting large unaxial anisotropy. This complex is formed from a tetradant ligand (hexathyl-2,2',2"-triamino-triethylamine) with three Nitrogens forming in plane bonds with the metal ion, the fourth Nitrogen forms a bond in the perpendicular plane as shown on figure

3.3. At the opposite of this fourth Nitrogen a halide apical ligand is found, Chlorine or Bromine.

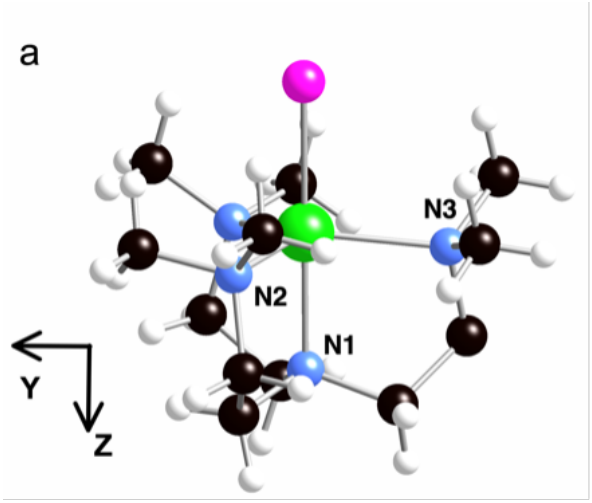

Figure 3.3: Representation of the complex [Ni(Me6trenCl)](ClO4), Ni in green, Cl, N in blue, C in black and H in white

Cristallographic data indicates that this complex crystallises in the trigonal space $R3c$ with a C_3 axis of symmetry along the Ni-Cl axis. This coordination induces a degeneracy of the d-orbital which share the same angular component m_l, *i.e* $d_{xy}(dxz)$ and $d_{x^2-y^2}(d_{yz})$. Conditions for 1^{st} order SOC are met between two degenerate ground state carried by the two d^8 configurations depicted on figure 3.4 This would result in a large splitting of the M_S component of the ground state with a large value for the D term as strong as the spin orbit coupling constant of the nickel ion (ξ_{Ni}=644cm^{-1}). At this stage, a competiting effect appears, the Jahn-Teller effect which break the orbital degeneracy by deforming the ligand which in turn reduces the axial anisotropy and give rise to non-zero rhombic term (E≠0). This distortion is confirmed by both eletron paramagnetic resonance (EPR) studies and theoretical study, this revokes the possibility of 1^{st}order SOC leaving only 2^{nd}order SOC at the origin of the anisotropy.

The ground state is now mainly carried by the configuration shown on figure 3.4 where the $d_{x^2-y^2}$ is simply occupied while the d_{xy} stays doubly occupied. The concluding remark of this study was that this complex shows a large axial anisotropy with $D \approx -120cm^{-1}$ and a significant rhombic term E=1.6cm^{-1}. While the Jahn-Teller effect has a large impact on the values of the D paramter, it is not able to completely negate it showing that the ligand rigidity is on par with the distortion.

The focus of our study lies in the interest of controlling the anisotropy via an external stimulus such as an electric field. Indeed, while the effect of magnetic field on the different M_S component is well known with the Zeeman Effect, it is practically impossible to focus a magnetic field at the nanoscale. This is not the case for electric field which allows very accurate control at this scale and can affect the magnetic properties of a material via Magneto-Electric couplings. *Ab initio* calculations allow for the appreciation of the Jahn-Teller distortion as well a the determination of the

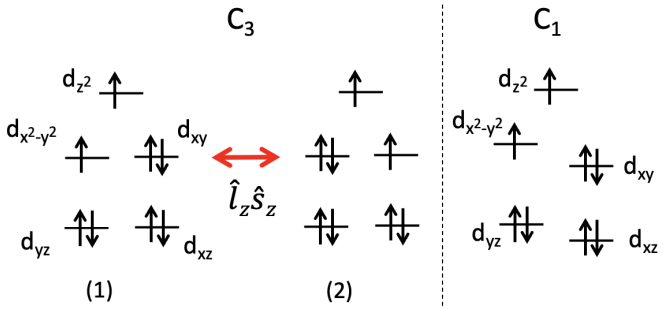

Figure 3.4: Energy diagrams of the d orbitals in case of three-fold symmetry C_3 (left) and in presence of Jahn-Teller distortion (right) with the induced lift of degeneracy of the d-orbitals.

anisotropic parameters D and E as a function of the applied electric field. The rationalization of such mechanism comes from the analysis of the spin-orbit coupled wave-function and the contribution of the excited states to the ZFS both provided by the ORCA program. The origin of this Magneto-Electric effect is believed to come from both electronic and geometric structure changes under the applied electric field. To identify and quantify these mechanisms, the electric field was applied under two different orientations in three types of calculations:

(a) eletronic structure changes, ZFS calculation under an applied field on the zero-field geometry

(b) geometric structure changes, ZFS calculation under no applied field on the field-optimised geometry.

(c) combined eletronic and geometric, both geometry optimisation and ZFS calculation performed under an applied electric field

To explore the different response to the electric field given its orientation, the field F was first applied along the Ni-Cl axis that corresponds to the easy axis of magnetization. This orientation include the maximal component of the dipole moment and will be referred as F//Z. It was then applied in a perpendicular direction (F//Y) in the YZ plane that include the Ni, N1 and N3 atom (refer to figure 3.3 for numerotation of atoms). This axis was chosen as the Ni-N3 bond length is the shortest among the three Ni-N bonds in the XY plane.

Analysis of the contribution

The main contribution to the D term comes from the SOC with the first excited triplet state (T^1) which is mainly expressed on the determinant created by exciting an electron occupying the $d_{x^2-y^2}$ to the d_{xy}. The Hamiltonian used to rationalize the SOC is given by $\hat{H}^{SO} = \sum_i \zeta(\hat{l}^i_x\hat{s}^i_x + \hat{l}^i_y\hat{s}^i_y + \hat{l}^i_z\hat{s}^i_z)$ where i runs over all the electrons of the d^8 configuration. The two lowest triplet are formed primarily from orbitals that are combination of m_l=±2, the resulting SOC then originate only from the $\hat{l}^i_z\hat{s}^i_z$ part of

the Hamiltonian between the m_s=±1 of each triplet. This coupling tends to stabilise the m_s=±1 of the T_0 ground state without affecting the m_s=0 component, which gives a negative contribution to the D term. This contribution can be estimated at second order perturbation:

$$C(D)^{(2)} = -\frac{|\langle T^0_{\pm 1}| \hat{H}^S O |T^1_{\pm 1}\rangle|^2}{\Delta E} \tag{3.2.1}$$

With $\Delta E = E(T^1) - E(T^0)$ being the energy difference between the two states. As the difference in energy is relatively small, a better treatment of this contribution can be obtained variationally by diagonalizing the 2×2 SOC matrices in the basis of $T^0_{\pm 1}$ and $T^1_{\pm 1}$:

$$C(D)_{VAR} = \frac{\Delta E - \sqrt{\Delta E^2 + 4|SOC|^2}}{2} \tag{3.2.2}$$

Where $|SOC|^2$ is the square value of the off-diagonal term in $\hat{H}^{SO}$ between ground and excited components. Other states may contribute positively or negatively to the overvalue value of D, their contribution can be obtained the same way. These contributions are also provided by the ORCA program, to approach the actual value of D one needs to sum all these contributions. However the variation of the electric field has almost no impact on the contributions from the excited state other than $T^1_{\pm 1}$, as such they will be left out of the rationalization. A rationalization of the rhombic term E will be done but as the sum of the contributions provided by the program do not match the overall variation of the E term the analysis will be done using the wave-function

3.2.1 Computational Informations

Wave function based calculations have been performed using the ORCA package. In a first place, Complete Active Space Self-Consistent Field calculations have been performed to account for non-dynamic correlations. The CAS(8,5) active space contains 8 electrons in the 5 essentially 3d orbitals of the Ni(II) ion, and two sets of orbitals have been optimized using an average procedure over all triplet and all singlet states of the configuration. To account for dynamic correlations at the 2nd order of perturbation, NEVPT217 calculations have been carried out for all states. The Spin-orbit State-Interaction method was then used to account for Spin-Orbit Couplings SOCs between the Ms components of all spin states using the NEVPT2 correlated energies as diagonal elements of the SO matrix. ZFS parameters were extracted using a procedure18 based on the effective Hamiltonian theory which proved to provide accurate values of the anisotropic parameters. The QZVPP extended basis sets21 have been used for Ni atoms (14s10p5d4f2g), SVP for H (2s1p) and TZVP for all other atoms (6s3p2d1f for N, 8s4p2d1f for Cl and 6s3p2d1f for C). As the field may change the geometrical structure, geometry optimizations were performed for different values and orientations of the field. We used the Hay-Wadt LanL2TZ(f) basis set for Ni and its corresponding relativistic effective core, Pople triple-ζ basis set (6-311G) for N24 and Cl25 atoms, a Pople double-ζ plus polarization basis set (6-31G*)26 for C atoms, and a Pople double-ζ basis set (6-31G) for H atoms26 and the B3LYP functional. Convergence thresholds for geometry optimization were set as VERYTIGHT.

The field will be applied in the two opposite directions referred as positive +F and negative –F with a maximal amplitude of |F|= 1.028.109 V.m-1. The positive direction for the field in the Z direction induces an elongation of the Ni2+-Cl- bond, i.e., the positive region of the electric potential is above Cl- in Figure 1. The positive direction for the field in the Y direction induces an elongation of the Ni2+-N3, i.e., the positive region of the electric potential is to the right of N3 in Figure 3.3.

3.2.2 Application of the electric field along the Z axis

First we consider the field F along the Z axis, which carry the main component of the dipole moment. Table 3.1 shows the three compoments of the dipole moment and its magnitude, while not perfectely aligned, most of the component is along the Z axis coinciding with the Ni-Cl bond while the X and Y component are small.

	μ_X	μ_Y	μ_Z	$\|\mu\|$
F=0	-0.0228007	-0.0772935	-8.1053645	8.1057651

Table 3.1: Dipole moment in Debye at F=0

Figure 3.5 shows the energy of the ground state as a function of the electric field for the three cases of calculation.

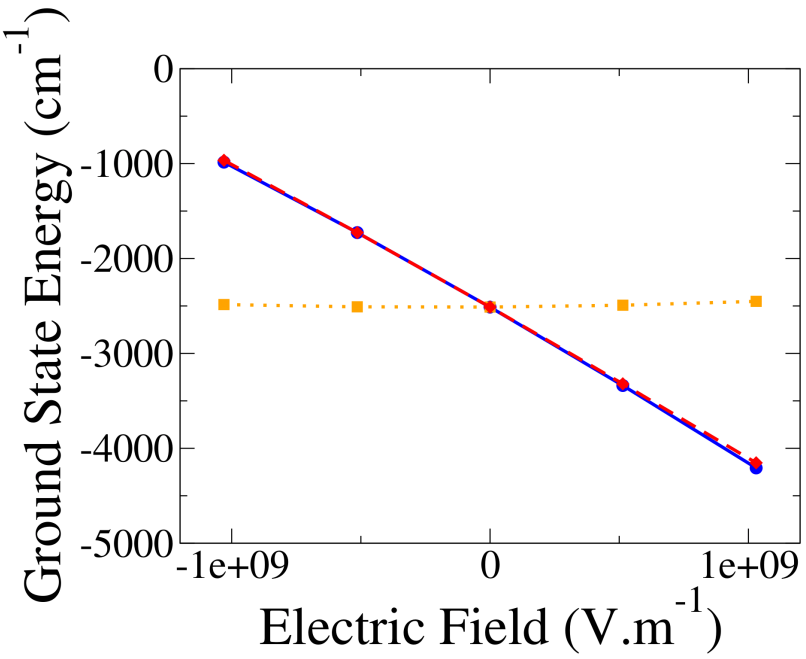

Figure 3.5: Energies in cm-1 (shifted by 58.35795.107 cm^{-1}) of the ground state obtained for the cases (a) (in blue and plain line), (b) (in orange and dotted line) and (c) (in red and dashed line) as functions of the field applied in the Z direction.

The variation of case (a) is linear with reference to the field F as expected from Stark

effect. In case (b) the energy follows a parabolic curves as the electric field is only a weak perturbation to the equilibrium geometry found a $F = 0V.m^{-1}$, the curvature being very small comapred to the variation from case (a) the overall behavior case (c) follows the eletronic effects (a).

Figure 3.6a shows the evolution of the D paramter as a function of the applied field F. In all three case the absolute variation $|dD/dF|$ is linear, with a negative slope in case (a) and positive in (b) and (c). This shows that the geometric effects (b) have a stronger effect that the electric ones (a) on the variation of the D value. The evolution of the E parameter is represented on figure 3.6b, even through some deviation is observed for the geometric case (b), mainly due to the lack of precision in calculating this specific property, the overall variation is linear to the field. Nonetheless the variation in case (b) is very small ($<$0.05 cm^{-1}) and the behavior of case (c) is now governed by the electronic effects with a negative absolute slope.

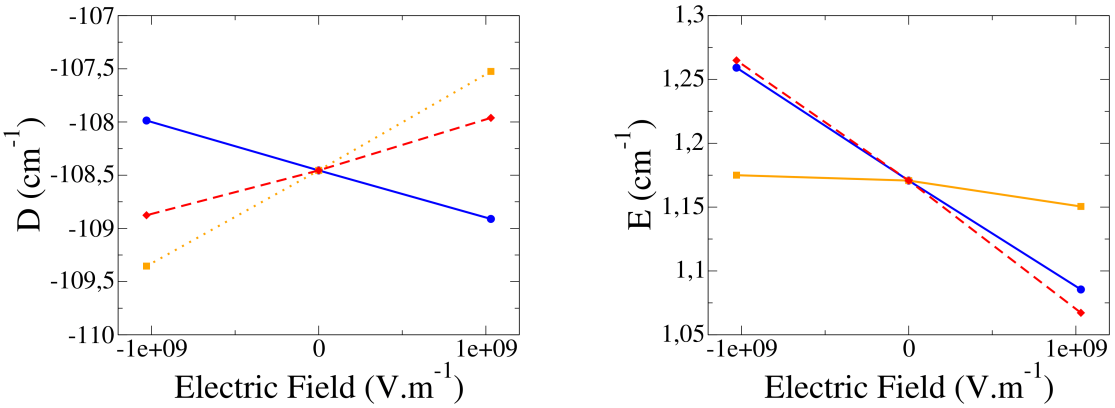

(a) Axial D parameter

(b) Rhombic E parameter

Figure 3.6: Evolution of the Axial D (left) and Rhombic E (right) parameters (in cm^{-1}) as a function of the field applied in cases (a) (in blue and plain line), (b) (in orange and dotted line) and (c) (in red and dashed line) in the Z

Table 3.2 shows the absolute slopes $|dD/dF|$ and $|dE/dF|$ in all three cases of calculations, note that these slopes are additive with good precision.

$Hz/(V.m^{-1})$	(a) Electronic structure	(b) Geometric structure	(c) Both	Sum of (a) and (b)
$\|dD/dF\|$	-13.52	+26.66	+13.15	+13.14
$\|dE/dF\|$	-2.53	-0.36	-2.88	-2.89

Table 3.2: Slopes of the straight lines in cases (a), (b) and (c) for the D and E parameter for F//Z

To rationalize these results, the most important contributions to the D parameter C(D) were studied as reported in table 3.3. As mentionned before, the main contribution comes from the first excited triplet, but it is also the most receptive contribution to the application of the field F with notable variation. Other states may have large contributions but small variation from $-F$ to $+F$, as these contribution are positive it

is clear that the first excited triplet is the main source of the large axial D parameter in this system.

	Excited state	**C(D) for -F**	**C(D) for +F**	$\Delta C(D)$ ORCA	$\Delta C(D)$ VAR.	$\Delta\|SOC\|^2$	$\Delta(\Delta E)$
(a)	T_1	-179.18	-180.06	-0.88	-0.82	1722.78	-1.60
	T_2	23.84	23.72	-0.12			
	T_3	19.61	19.68	0.07			
	S_3	20.48	20.57	0.09			
(b)	T_1	-180.95	-178.25	2.70	2.70	-209.90	36.2
	T_2	23.82	23.72	-0.10			
	T_3	19.71	19.58	-0.13			
	S_3	20.55	20.51	-0.04			
(c)	T_1	-180.49	-178.66	1.83	1.90	1509.15	34.7
	T_2	23.88	23.66	-0.22			
	T_3	19.67	19.61	-0.06			
	S_3	20.51	20.56	0.05			

Table 3.3: Contributions to the axial parameter D (in cm-1) of the most contributing excited states and their variations ΔC(D) between the -F and +F in the Z direction either provided by ORCA or calculated variationally. Δ|SOC|2 is the variation of the square of the module of the SOC between the ground and the first excited triplet states while Δ(ΔE) is the variation between the -F and +F of their energy difference (in cm^{-1}) obtained at the NEVPT2 level.

The variation of the first excited triplet $\Delta C(D)_{VAR}$ matches well with the one provided by ORCA indicating that one can use the variation of the SOC as well as the variation of the difference in energy $\Delta(\Delta E)$ for the analysis. Perturbative estimation of this contribution gives a slightly larger contribution ($-193cm^{-1}$ at $F = 0$) because the two lowest states are rather close in energy ($\approx 2166cm^{-1}$) leaving the pertubation regime. In case (a), the difference in energy between the two lowest triplets states remain roughly the same leaving the variation of SOC as the leading factor in the change of $|D|$, as the soc increases so does D. The opposite is seen in case (b) where the leading factor is the change in energy of the two states. The energy difference increases thus $|D|$ decreases as can be deduced from the perturbative expression of the contribution 3.2.1. The overall changes in $|D|$, case (c), follow the same behavior as case (b) as the energy difference remains the leading factor indicating that the geometrical structure dominates. This can be explained by the geometry changes under the application of

Ligands	$-F$	$+F$	$\Delta(distance)$
Cl	2.31391	2.32709	$131.8.10^{-4}$
N_1 (apical)	2.2.15016	2.14727	$-28.9.10^{-4}$
N_2	2.22739	2.22043	$-69.6.10^{-4}$
N_3	2.14628	2.14139	$-48.9.10^{-4}$
N_4	2.22688	2.22023	$-6.65.10^{-4}$

Table 3.4: Variation of the distances in Angstrom between the Ni(II) ion and the closest atoms of the ligand between $-F$ and $+F$ with F//Z.

the eletric field reported in Table 3.4 with the variation of the distances between the Ni(II) ion and its coordination sphere between $+F$ and $-F$. The Ni-Cl bond length

increases with positive field $+F$, as this bond carries most of the dipole moment it is expected to lenghten in order to maximize its interactions with the field. However, all the others atoms tend to move closer to the Ni(II) ion which increases the ligand field in the XOY plane.

This destabilise both the $d_{x^2-y^2}$ and d_{xy}, the former pointing directly toward N_3 is more affected, leading to an increase in the energy difference between these orbitals and thus between the ground and excited state. As we can see from Table 3.3 and 3.5, the variation of the two difference in energy follow the same behavior in each case of calculation.

Variation of the orbital energy differences	(a)	(b)	(c)
$\Delta(\Delta\epsilon(d_{x^2-y^2} - d_{xy}))$	6.58	258.98	267.76

Table 3.5: Variation between $-F$ and $+F$ applied in the Z direction of the orbital energy difference $\Delta(\Delta\epsilon(d_{x^2-y^2} - d_{xy}))$ in cm^{-1}

The rhombic term E describes the difference in anisotropy between the X and Y axis, for its rationalization one would want to apply the same analysis as the D term based on the contributions provided by ORCA. Unfortunately these contributions cannot be used because their sum increases with the field while the E values extracted via effective Hamiltonian theory decrease as represented on figure 3.6b. Nevertheless it is possible to rationalize the E term by identifying the determinants that distinguish the X from the Y direction. In the case of an applied field along the Z axis, the $d_{x^2-y^2}$,d_{xy} and d_{z^2} are symmetric in X and Y, as such the only determinants that treat differently these two directions are those with a single occupation in the d_{xz} or d_{yz}. There are six of these determinants with M_S=1, two of them have the largest coefficients in the wave-function of the T_2 and T_3 excited states and are results of single excitation from either of these orbitals to the $d_{x^2-y^2}$ or d_{z^2} which are singly occupied in the ground state T_0. If there is no difference between the two directions, *i.e* no rhombicity E=0, the weights of these determinants should be the same in both states leading to two contributions that cancel out. To estimate the evoluton of the rhombicity, one can look at the variations of these weight with respect to the field. Let's define $\Delta w(X-Y)$ which is the difference between the weight w(d_{xz}) and w(d_{yz}) and its overall variation $\Delta(\Delta w(X-Y))$ between $+F$ and $-F$ as reported in Table 3.6.

First, we can notice the small variation for case (b) which matches well the variation of E for this case in 3.6b. The variation $\Delta(\Delta w(X-Y))$ is very similar between case (a) and case (c), this confirms that the overall variation of the E term is dictated by the electronic structure changes induced by the application of the electric field.

3.2.3 Application of the electric field along the Y axis

Now, let's consider the applied field along the Y direction F//Y, the field is now perpendicular to the main component of the dipole moment (μ_Z). Note that the field is not directly applied along the Ni-N_3 bond as it is slightly ouut of the XoY plane, the reason for that is that it made sense to consider two perpendicular orientation onto which apply the electric field Figure 3.7 shows the evolution of the ground state energy

		$-F$	$-F$	$\Delta(\Delta w(X-Y))$
(a)	$w(d_{xz})$	96.200	96.741	-0.528
	$w(d_{yz})$	97.210	97.224	
	$\Delta w(X-Y)$	1.010	0.482	
(b)	$w(d_{xz})$	96.543	96.494	0.088
	$w(d_{yz})$	97.282	97.145	
	$\Delta w(X-Y)$	0.739	0.651	
(c)	$w(d_{xz})$	96.271	96.762	-0.621
	$w(d_{yz})$	97.282	97.152	
	$\Delta w(X-Y)$	1.011	0.390	

Table 3.6: Weight w(d_{xz}) and w(d_{yz}) of the determinants with single occupation in the respective orbitals, their difference $\Delta w(X-Y)$ and their overall variation $\Delta(\Delta w(X-Y))$ in all three case of calculation.

when F//Y, the quadratic behavior of the case (a) curve can be explained by a change in sign of the dipole moment component μ_Y

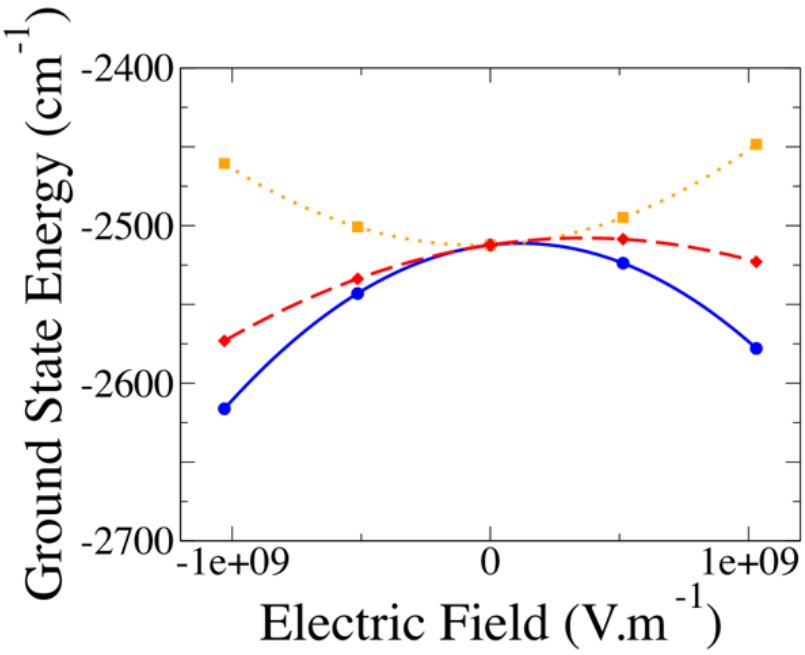

Figure 3.7: Energies in cm-1 (shifted by 58.35795.107 cm^{-1}) of the ground state obtained for the cases (a) (in blue and plain line), (b) (in orange and dotted line) and (c) (in red and dashed line) as functions of the field applied in the Y direction.

Figure 3.8a shows the evolution of the D term with respect to the applied field, it once again follows a linear behavior in all three cases. The sign of the slopes now have inversed with $|dD/dF|$ being positive for case (a) and negativ for both case (b) and (c) as opposed to when the field was along the Z direction.

The slopes for each case are shown in Table 3.7, once again the variation of the D

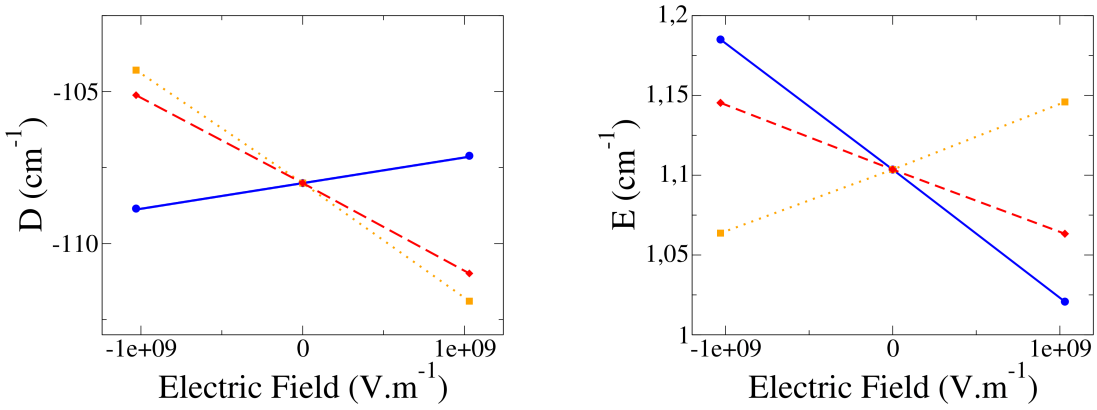

(a) Axial D parameter

(b) Rhombic E parameter

Figure 3.8: Evolution of the Axial D (left) and Rhombic E (right) parameters (in cm^{-1}) as a function of the field F//Y in cases (a) (in blue and plain line), (b) (in orange and dotted line) and (c) (in red and dashed line)

term is dictated by the geometrical changes under the applied field, case (b). Note that the slopes $|dD/dF|$ are very much additive and now much higher in the case F//Y than it was with F//Z, almost seven times larger.

$Hz/(V.m^{-1})$	(a) Electronic structure	(b) Geometric structure	(c) Both	Sum of (a) and (b)
$\|dD/dF\|$	+25.32	-110.75	-85.45	-85.43
$\|dE/dF\|$	-2.39	+1.20	-1.19	-1.19

Table 3.7: Slopes of the straight lines in cases (a), (b) and (c) for the D and E parameter for F//Y

The same rationalization can be applied here through the evolution of the ligand field. The application of the field al the

Ligands	$-F$	$+F$	$\Delta(distance)$
Cl	2.32024	2.32043	$2.4.10^{-4}$
N_1 (apical)	2.14947	2.14727	$1.7.10^{-4}$
N_2	2.22518	2.22245	$-27.3.10^{-4}$
N_3	2.1482	2.14596	$11.4.10^{-4}$
N_4	2.2270	2.22229	$-4.1.10^{-4}$

Table 3.8: Variation of the distances in Angstrom between the Ni(II) ion and the closest atoms of the ligand between $-F$ and $+F$ with F//Y.

Chapter 4

Electric field on Exchange anisotropy

Numerous studies have been conducted to characterise certain properties of magnetic anisotropies and many procedures have been developped with great success as discussed above. However, only a few studies have been applied to determine the properties of the exchange anisotropy using Quantum Chemistry theories. This study is part of a series of work that aims to rationalize the origin of exchange anisotropy in polynuclear molecules. The spin Hamiltonian used to describe anisotropic behavior in binuclear systems is as follows:

$$\hat{H}_{AB} = J_{AB}\hat{\mathbf{S}}_A \cdot \hat{\mathbf{S}}_B + \hat{\mathbf{S}}_A \cdot \overline{\overline{D}}_{AB} \cdot \hat{\mathbf{S}}_B + \mathbf{d}_{AB} \cdot (\hat{\mathbf{S}}_A \times \hat{\mathbf{S}}_B) \tag{4.0.1}$$

In order to achieve this, a procedure of extractin was developped to obtain values of the Dzyaloshinskii-Moriya pseudovector interaction as well as the symmetric exchange anisotropy D_{ij}-tensor using effective Hamiltonian theory in combination with wave-funcion based method.

This procedure was tested on a simple model molecule represented on figure 4.1 which consists of two Cu^{2+} cations separated by Cl^{-} anions.

This choice of this system lies in its simplicity, with only one magnetic electron per center and a reasonnable size it allows for simple analytical derivation and high level treatment of the correlation. Such a toy molecule can also be modeled to assess the impact of geometry, *i.e* distances and angles, on these interactions. It was first determined that the most favourable setting for obtaining large values of anisotropic interaction is to approach first order coupling regime without reaching it. Such situation arises when the outside angle ϕ reaches 120°, the local environment of each Cu^{2+} is then close to a C_3-axis symmetry. This allow the condition of quasi-degeneracy of the $d_{x^2-y^2}$ and d_{xy} orbitals to be achieved, but due to the D_{2h} symmetry of the system it possess an inversion center leading to a zero value of DMI. To induce a non-zero value of the DMI, the first two studies relied on the deformation of the molecule via a variation of the θ angle resulting in the hybridization of the otherwise pure cartesian d-orbitals. This mixing of the d-orbital is the key ingredient to the creation of DMI, as it was shown that increasing the mixing allow for the obtention of very large values of DMI. It was then though that the application of an external electric field could have the same effect with a smaller scale by acting not on the nuclei's position but the

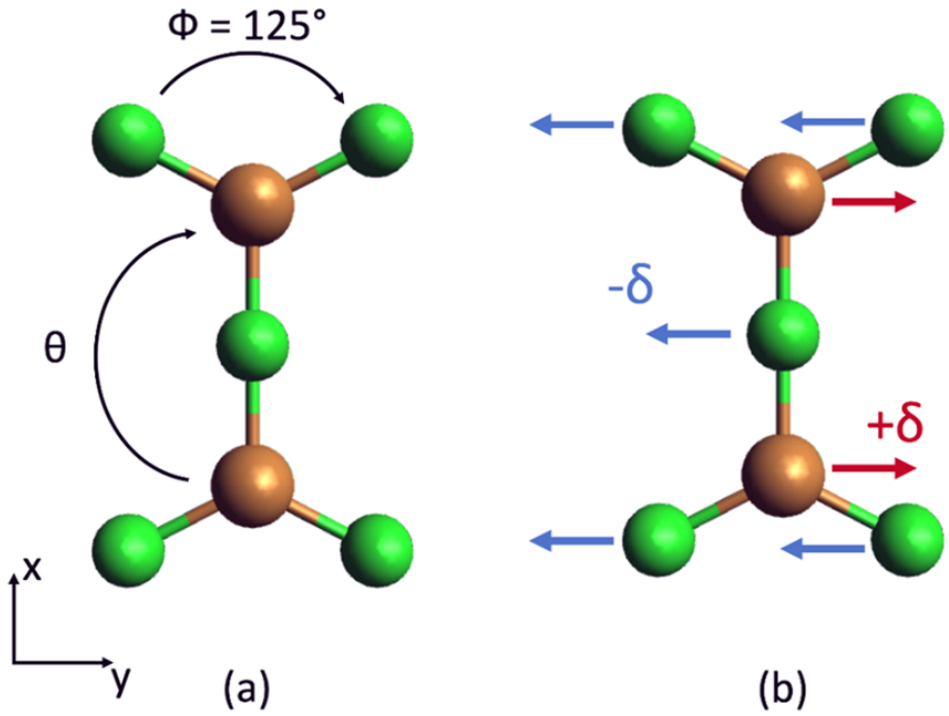

Figure 4.1: (a) Cu_2Cl_5 model molecule of D_{2h} symmetry, (b) displacement δ of the atoms generated by the application of an electric field along the y direction.

electronic cloud itself. As mentionned in the previous chapter, an electric field is a very interesting choice to consider as it can be focused accurately at the molecular level. It is also much easier to use an external stimuli instead of relying on the "intrinsic" geometry of the molecule. In a following work, the impact of the electric field on the isotropic and antisymmetric exchange spin Hamiltonian parameter was determined, it was determined that the Dzyaloshinskii-Moriya pseudo-vector is very sensitive to the external field. Here we follow the already established procedure to focus our attention on the symmetric exchange anisotropy tensor. The work follows to two axis:

(i) Derive an appropriate model to estimate the symmetric tensor in the condition of 1^{st} order SOC in the absence of electric field.

(ii) Study the variation of the symmetric tensor under the effect of the electric field and its behavior relative to the DMI.

4.1 Computational Informations

The computation of the eletronic and relativistic states were performed on the MOLCAS code. Complete-Active-Space-Self-Consistent field calculations were carried out for various values angle Φ ranging from $\Phi = 130°$ (close to 1^{st} order SOC) to 170° (far from it). The active space consists in the six electrons occupying the $d_{x^2-y^2}$ and d_{xy} orbitals of each copper center, CAS(6,4) with two set of orbitals optimised in an average

way, one for the four lowest triplet and the other for the four lowest singlet states. The enlarge active space containing all d-orbitals and their electrons, CAS(18,10) was also considered but previous study showed that it had little impact on the extracted paramaters and that the reduce active space CAS(6,4) was enough to capture the effect of first order SOC. It was nonetheless used for the treatment of second order spin orbit coupling.

Dynamical correlation was introduced using the Difference-dedicated-configuration-interaction (DDCI3) method perfored via the CASDI code interfaced with the MOLCAS chain. Three type of SO-SI calculations were performed:

(i) CAS(6,4)SCF : the energy and wavefunction are obtained from CASSCF calculation

(ii) CAS(6,4)DDCI/SCF-SO : the DDCI energy are used while the wavefunction remain that of the CAS(6,4)SCF

(iii) CAS(6,4)DDCI/DDCI-SO : the energy and wavefunction are obtained from DDCI calculation

This allows to study the impact of each component of dynamic correlation (energy or wavefunction) on the exchange interactions. The TZVP basis set were used throughout all calculations: 5s4p3d1p for Cu and 4s3p1d for Cl.

The continious electric field was added in the SEWARD stage of the calculation in MOLCAS, the X,Y and Z directions were treated but most of the results reported here relates to the Y direction.

4.2 Theorical model

To derive the parameters of the Multispin Hamiltonian, we first have to define the model space. Let's call a (a') and b(b') the magnetic orbitals located on each copper ion, these orbitals are obtained from state specific calculation and might differ between triplet and singlet states by the tails on the Cl^- ligands hence the difference of notation a and a'. One can predict that with the application of an electric field, the otherwise pure cartesian orbitals $d_{x^2-y^2}$ and d_{xy} will hybridize to form the orbital $a(a')$ and $b(b')$. We note the orthogonal cartesians orbitals $a_1(b_1)$ and $a_2(b_2)$ respectively depending on the site A or B.

$$a = \alpha a_1 + \beta a_2 \qquad b = -\alpha b_1 + \beta b_2 \qquad a' = \alpha' a_1 + \beta' a_2 \qquad b' = -\alpha' b_1 + \beta b_2 \quad (4.2.1)$$

Where $\alpha(\alpha')$ and $\beta(\beta')$ are the mixing coefficients between the d orbital in the triplet(singlet) state. The coupling between the lone electron of each copper ion gives rise to a triplet

and singlet state that will form the basis of the model space:

$$T^{+} = |ab| \tag{4.2.2}$$

$$T^{0} = \frac{1}{\sqrt{2}}(|a\overline{b'}| - |b\overline{a'}|) \tag{4.2.3}$$

$$T^{-} = |\overline{a}\overline{b}| \tag{4.2.4}$$

$$S = \frac{1}{\sqrt{2}}(|a'\overline{b'}| + |b'\overline{a'}|) \tag{4.2.5}$$

The matrix representation of the Multi-Spin Hamiltonian in this basis is:

H_{MS}	T^{+}	T^{0}	T^{-}	S
T^{+}	$\frac{J_{AB}}{4} + \frac{D_{zz}}{4}$	$\frac{D_{xz}-iD_{yz}}{2\sqrt{2}}$	$\frac{(D_{xx}-D_{zz}-2iD_{xy})}{4}$	$\frac{d_y+id_x}{2\sqrt{2}}$
T^{0}	$\frac{D_{xz}+iD_{yz}}{2\sqrt{2}}$	$\frac{J_{AB}}{4} - \frac{D_{zz}}{4} + \frac{(D_{xx}+D_{yy})}{4}$	$-\frac{D_{xz}-iD_{yz}}{2\sqrt{2}}$	$-\frac{id_z}{2}$
T^{-}	$\frac{(D_{xx}-D_{zz}+2iD_{xy})}{4}$	$-\frac{D_{xz}+iD_{yz}}{2\sqrt{2}}$	$\frac{J_{AB}}{4} + \frac{D_{zz}}{4}$	$\frac{d_y-id_x}{2\sqrt{2}}$
S	$\frac{d_y-id_x}{2\sqrt{2}}$	$\frac{id_z}{2}$	$\frac{d_y+id_x}{2\sqrt{2}}$	$-\frac{3J_{AB}}{4} - \frac{D_{zz}}{4} - \frac{(D_{xx}+D_{yy})}{4}$

The evolution of the J_{AB} the isotropic coupling and the component d_x, d_y and d_z under the application of an external electric field has already been studied previously. The component D_{xx}, D_{xy},etc are the component of the symmetric exchange anisotropy $\overline{\overline{D}}$-tensor which is the focus of this study and its evolution will be compared to previous results, especially with the DMI.

Approaching the condition of quasi-degeneracy of the $d_{x^2-y^2}$ and d_{xy} orbitals, *i.e* first order spin orbit coupling, the use of second order perturbation theory is now impossible to account for spin-orbit coupling because of the small differences in energy between the lowest states. As such, variational treatment is mandatory, to do so a model was derived to assess the contribution of 1^{st} order SOC based on the spin-free states generated by the occupation of these two orbitals. The following states form the uncoupled basis:

$$
\begin{aligned}
T_1^+ &= |a_1 b_1|; \qquad T_1^0 = \frac{|a_1\bar{b}_1| - |b_1\bar{a}_1|}{\sqrt{2}} \\
S_1 &= \frac{|a_1\bar{b}_1| - |b_1\bar{a}_1}{\sqrt{2}} \\
T_2^+ &= \frac{|a_1 b_2| + |b_1 a_2|}{\sqrt{2}}; \qquad T_2^0 = \frac{|a_1\bar{b}_2| + |b_1\bar{a}_2| - |a_2\bar{b}_1| - b_2\bar{a}_1|}{2} \\
S_2 &= \frac{|a_1\bar{b}_2| + |b_1\bar{a}_2| + |a_2\bar{b}_1| + b_2\bar{a}_1|}{2} \\
T_3^+ &= \frac{-|a_1 b_2| + |b_1 a_2|}{\sqrt{2}}; \qquad T_3^0 = \frac{-|a_1\bar{b}_2| + |b_1\bar{a}_2| - |a_2\bar{b}_1| + b_2\bar{a}_1|}{2} \\
S_3 &= \frac{-|a_1\bar{b}_2| + |b_1\bar{a}_2| + |a_2\bar{b}_1| - b_2\bar{a}_1|}{2} \\
T_4^+ &= |a_2 b_2|; \qquad T_4^0 = \frac{|a_2\bar{b}_2| - |b_2\bar{a}_2|}{\sqrt{2}} \\
S_4 &= \frac{|a_2\bar{b}_2| - |b_2\bar{a}_2|}{\sqrt{2}}
\end{aligned}
\tag{4.2.6}
$$

The ionic part of these states were left out of the model for simplicity but will be taken into account in the *ab inito* calculations as they play an essential part in the antiferromagtic coupling. Note that crystal field theory indicates that in absence of electric field, the magnetic orbitals are the $d_{x^2-y^2}$ on each copper center, thus the energy ordering should follow the same order they are expressed in 4.2.6. The Spin-Orbit matrix can be derived from the SO-Hamiltonian:

$$\hat{H}^{SO} = \zeta(\hat{l}_1\hat{s}_1 + \hat{l}_2 + \hat{s}_2) \tag{4.2.7}$$

With $\hat{l}_i$ the angular momenta and $\hat{s}_i$ the spin momenta operators working on electron i and ζ the spin-orbit constant. The spin-orbit couplings between the states 4.2.6 originate from the $\hat{l}_z\hat{s}_z$ part of the $\hat{H}^{SO}$ that couples the determinants formed from orbitals of same spatial (m_l) and spin (m_s) component. The representation matrix of this Hamiltonian in the basis developped in eq 4.2.6 with the addition of electronic couplings.

The electronic effect included are the isotropic couplings J_i between triplet and singlet states of same spatial nature. $h_i(h_i\text{'})$ coupling are induced by the mixing of the the $d_{x^2-y^2}$ and d_{xy} orbitals when the electric field is applied along the Y direction, this coupling is at the origin of the DMI interaction in this system as it opens coupling path between S_1 and T_1^0. Estimation of the couplings can be done perturbatively at second order, but as the system enter 1^{st} order SOC the best approach is to diagonalize the matrix. To understand the origins of the anisotropic parameter, D_{AB} and the DMI, the couplings must be decomposed by their contributions. Simply speaking, the D_{AB} describe the difference in energy between the M_S=$\pm$ 1 and the M_S=0 component. From

$\hat{H}^{SO}$	$\|T_1^+\rangle$	$\|T_2^+\rangle$	$\|T_3^+\rangle$	$\|T_4^+\rangle$	$\|T_1^0\rangle$	$\|T_2^0\rangle$	$\|T_4^0\rangle$	$\|S_1\rangle$	$\|S_3\rangle$	$\|S_4\rangle$
$\langle T_1^+\|$	E_1+J_1	h_1	$i\zeta\sqrt{2}$	δ_4	0	0	0	0	0	0
$\langle T_2^+\|$	h_1	E_2+J_2	0	h_2	0	0	0	0	0	0
$\langle T_3^+\|$	$-i\zeta\sqrt{2}$	0	E_3+J_3	$i\zeta\sqrt{2}$	0	0	0	0	0	0
$\langle T_4^+\|$	δ_4	h_2	$-i\zeta\sqrt{2}$	E_4+J_4	0	0	0	0	0	0
$\langle T_1^0\|$	0	0	0	0	E_1+J_1	h_1	δ_4	0	$-i\zeta\sqrt{2}$	0
$\langle T_2^0\|$	0	0	0	0	h_1	E_2+J_2	h_2	$-i\zeta\sqrt{2}$	0	$-i\zeta\sqrt{2}$
$\langle T_4^0\|$	0	0	0	0	δ_4	h_2	E_4+J_4	0	$-i\zeta\sqrt{2}$	0
$\langle S_1\|$	0	0	0	0	0	$i\zeta\sqrt{2}$	0	E_1	h_1'	δ_4'
$\langle S_3\|$	0	0	0	0	$i\zeta\sqrt{2}$	0	$i\zeta\sqrt{2}$	h_1'	E_3	h_2'
$\langle S_4\|$	0	0	0	0	0	$i\zeta\sqrt{2}$	0	δ_4'	h_2'	E_4

Table 4.1: Representation matrix of $\hat{H}^{SO}$ and electronic couplings in the uncoupled basis. T_3^0 and S_2 are not coupled to the others, as such they were left out for clarity. $h_1(h_1$') and $h_2(h_2')$ are couplings induced by the electric field and differ between triplet and singlet states by their exchange integrals. δ_1 and δ_2 are small bielectronic integrals between $T_1(S_1)$ and $T_4(S_4)$. The M_S=-1 components of the triplets are left out but possess the same couplings as the M_S=1 components.

this matrix there is no difference in couplings between the two M_S=$\pm$1, as such there is no rhombic term E_{AB} when considering only first order SOC, hence to estimate the D_{AB} one has to look for states coupled to T_1^0 or T_1^+. The T_1^+ component is coupled via SOC with T_3^+ which will stabilize it, contributing negatively to the D_{AB} by bringing down in energy the M_S=$\pm$1 component. On the other hand, the S_3 which is coupled to T_1^0 will bring a positive contribution to the D_{AB}. One way to assess their contribution is by diagonalizing the matrix with only the relevant couplings, T_3^+ or S_3, and see how the energies of T_1^+ or T_1^0 are affected. The small bielectronic integrals δ_4 and δ_4' also allow the contribution of T_4^+ and S_4 but to a much smaller scale.

In the presence of an electric field applied in the Y direction, the situation of table 4.1, the h_i and h_i' electronic coupling turn different from zero and new pathways open up for the DMI. As shown in matrix **??**, the d_z component is created by the coupling between the T_1^0 and the S_1 states which can be expressed using second order pertubation theory:

$$\frac{id_z}{2} = \langle S|\, H^{SO}\, |T^0\rangle^{(0)} = \frac{\langle S_1|\, H^{SO}\, |T_2^0\rangle\, \langle T_2^0|\, H^{el}\, |T_1^0\rangle}{E_2+J_2-E_1} + \frac{\langle S_1|\, H^{el}\, |S_3\rangle\, \langle S_3|\, H^{SO}\, |T_1^0\rangle}{E_3-E_1} \tag{4.2.8}$$

This equation is only valid far from first order SOC regime but helps visualising how the DMI appears due to the combination of electronic and spin orbit couplings.

To be complete in the extraction, one must also consider the effect of higher lying states made from determinant with the d_{xz} or d_{yz}, noted $a_3(b_3)$ and $a_4(b_4)$, singly occupied.

$$
\begin{aligned}
T_5^+ &= \frac{-|a_1 b_3| + |b_1 a_3|}{\sqrt{2}} \qquad T_5^0 = \frac{-|a_1\overline{b}_3| + |b_1\overline{a}_3| - |a_3\overline{b}_1| + |b_3\overline{a}_1|}{2} \\
S_5 &= \frac{-|a_1\overline{b}_4| + |b_1\overline{a}_3| + |a_3\overline{b}_1| - |b_3\overline{a}_1|}{2} \\
T_6^+ &= \frac{-|a_1 b_4| + |b_1 a_4|}{\sqrt{2}} \qquad T_6^0 = \frac{-|a_1\overline{b}_4| + |b_1\overline{a}_4| - |a_4\overline{b}_1| + |b_4\overline{a}_1|}{2} \\
S_6 &= \frac{-|a_1\overline{b}_4| + |b_1\overline{a}_4| + |a_4\overline{b}_1| - |b_4\overline{a}_1|}{2}
\end{aligned}
\tag{4.2.9}
$$

These states are coupled with T_1 and S_1 through the $\hat{l}_+\hat{s}_- + \hat{l}_-\hat{s}_+$ operator in $\hat{H}^{SO}$. Note that the determinants formed from the d_{z^2} orbital can be left out because it cannot interact with either T_1 or S_1 via $\hat{H}^{SO}$. Taking these states into account able to differentiate the two M_S=±1 of the triplet state and create a rhombicity in the

4.3 Impact of First Order Spin Orbit Coupling in the absence of electric field

The symmetric anisotropic exchange is described by a tensor of rank two which has six different components in a random set of axis. Expressed in its proper axis this is reduced to simply two, an axial parameter D_{AB} and rhombic term E_{AB}. Expression for these term have already been derived using second order perturbation theory and involves the $T_5(S_5)$ and $T_6(S_6)$ states:

$$
\begin{aligned}
D_{AB} &= 4\frac{\zeta^2 J_3}{\Delta E_3^2} - \frac{1}{2}\left(\frac{\zeta^2 J_5}{\Delta E_5^2} + \frac{\zeta^2 J_6}{\Delta E_6^2}\right) \\
E_{AB} &= \frac{1}{2}\left(\frac{\zeta^2 J_5}{\Delta E_5^2} - \frac{\zeta^2 J_6}{\Delta E_6^2}\right)
\end{aligned}
\tag{4.3.1}
$$

where $\Delta E_i^2 = \sqrt{\Delta T_i \Delta S_i}$ is the geometric mean of excitation energy between the state T_1 and T_i or S_i and $J_i = E_{T_i} - E_{S_i}$ is the isotropic coupling between excited states. As the first term of D_{AB} in eq 4.3.1 involves a state that contributes to 1^{st} order SOC, its estimation might deteriorate as ϕ decreases, *i.e* entering first order regime. This render these equation valid only far from first-order regime and in absence of external field. Note that the rhombic term requires the inclusion of the higher states to be different from zero.

To perform a rigorous extraction of the anisotropic parameter would require to include all the excited state generated from single excitation within the d-orbital space, *i.e* CAS(18,10). As this work focus solely on the contribution of 1^{st} order SOC, a CAS(6,4) is enough. To assess the impact of dynamical correlation on the D_{AB} parameter, calculations were performed with gradual inclusion of the DDCI3 components (energy and wave-function). These results are reported on figure 4.2 with the angle ϕ variating from 130° to 170°.

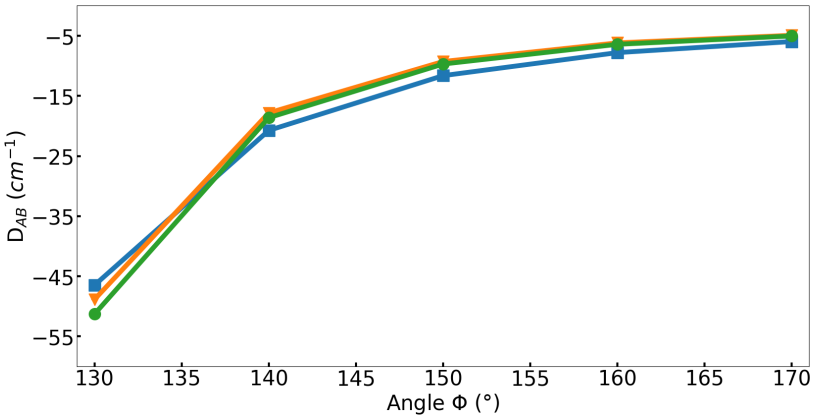

Figure 4.2: D_{AB} as a function of the outside angle ϕ for (i) CAS(6,4)SCF/SCF-SO level (blue line with squares), (ii) CAS(6,4)DDCI/SCF-SO level (orange line with triangles), and (iii) CAS(6,4)DDCI/DDCI-SO level (green line with circles)

This shows that the magnitude $|D_{AB}|$ increases when entering 1^{st} order SOC, *i.e* a decrease of the angle ϕ. A similar observation has been made for the DMI in previous study and in mononuclear complexes for local zero field splitting parameter D. It is important to observe that far from first order SOC, the impact of electron correlation is not very important with only a slight variation between the three curves. This difference increases when ϕ decreases. Note that the curves (ii) and (iii), which differ by the wave-function used (CASSCF-SO or DDCI-SO) are very similar and that the inclusion of the DDCI wavefunction does not improve the results much unlike what was observed with the DMI. Hence the us of the correlated DDCI wave-function in addition to the DDCI energies is not required and CASSCF wave-function should suffice in the SO-SI calculation in absence of DMI. As the rest of this work include a DMI, which has been proven to require the DDCI wave-functions, we have considered the CAS(6,4)DDCI/DDCI-SO calculation for numerical estimates.

Far from first order SOC the equation 4.3.1 can be used with the large active space CAS(18,10) taking into account the states 4.2.9. At $\phi = 170°$, the perturbative espressions give D_{AB}^{pert}=-4.86cm^{-1} and E_{AB}^{pert}=0.18cm^{-1}, a good estimate when compared to the value extracted from the CAS(18,10)DDCI/DDCI-SO and effective Hamiltonian theory D_{AB}=-4.09cm^{-1} and E_{AB}=0.10cm^{-1}. The slight overestimation may come from the fact that a unique $\zeta = 830cm^{-1}$ value of the free ion Cu^{2+} was used, in a complex this value is bound to decrease. These expressions lose their quality when entering first order SOC as expected, $\phi = 130°$, D_{AB}^{pert}=-83.31cm^{-1} and E_{AB}^{pert}=0.21cm^{-1} compared with the values extracted from CAS(18,10)DDCI/DDCI-SO and effective Hamiltonian theory D_{AB}=-45.20cm^{-1} and E_{AB}=0.02cm^{-1}. The rhombicity is almost naught justifying the use of the small active space CAS(6,4) compared to the CAS(18,10).

The matrix 4.1 was extracted from ab initio calculation, CAS(6,4)DDCI/DCCI-SO at $\phi = 130°$ and no electrical field, its numerical matrix is shown in table 4.2 with good correspondance. Note that the coupling terms h_i are equal to zero making it impossible

$\hat{H}^{SO}$	$\|T_1^+\rangle$	$\|T_2^+\rangle$	$\|T_3^+\rangle$	$\|T_4^+\rangle$	$\|T_1^0\rangle$	$\|T_2^0\rangle$	$\|T_4^0\rangle$	$\|S_1\rangle$	$\|S_3\rangle$	$\|S_4\rangle$
$\langle T_1^+\|$	1585	0	1079i	12	0	0	0	0	0	0
$\langle T_2^+\|$	0	2362	0	0	0	0	0	0	0	0
$\langle T_3^+\|$	-1079i	0	3275	1079i	0	0	0	0	0	0
$\langle T_4^+\|$	12	0	-1079i	5036	0	0	0	0	0	0
$\langle T_1^0\|$	0	0	0	0	1585	0	12	0	-1078i	0
$\langle T_2^0\|$	0	0	0	0	0	2362	0	-1075i	0	-1076i
$\langle T_4^0\|$	0	0	0	0	12	0	5036	0	-1078i	0
$\langle S_1\|$	0	0	0	0	0	1075i	0	550	0	2
$\langle S_3\|$	0	0	0	0	1078i	0	1078i	0	3369	0
$\langle S_4\|$	0	0	0	0	0	1076i	0	2	0	4486

Table 4.2: Numerical matrix of $\hat{H}^{SO}$ and electronic couplings in the uncoupled basis from a CAS(6,4)DDCI/DDCI-SO calculation with no electric field and $\phi = 130°$.

	D_{AB}
Contribution of T_3^+ and T_3^-	-1176.74
Contribution of S_3	1124.28
Sum	-52.46
D_{AB} from H^{eff}	-52.46

Table 4.3: Variational contribution in cm^{-1} of the excited states to D_{AB} and its value in cm^{-1} extracted from effective Hamiltonian at CAS(6,4)DDCI/DDCI-SO level

for DMI to occur. Diagonalizing this matrix with or without the inclusion of T_3^+ and S_3 allow to determine their individual contribution to the D_{AB} which are reported in table 4.3 The sum of the two contributions matches perfectely with the value obtained via H^{eff}.

Note that from the final value of D_{AB} and the perturbative expression 4.3.1, it is clear that the main contribution to the D_AB comes from T_3 and S_3 even with the large active space CAS(18,10) justifying once again the use of the small CAS(6,4) calculations.

4.4 Impact of the electric field on the symmetric anisotropic exchange parameter

This section focus on the bahavior of the anisotropic parameter in first order spin orbit coupling, $\phi = 130°$, in the presence of an applied external electric field. Only the changes in electronic structure are studied and not the geometric ones, indeed a previous study showed that the geometric changes only affected the values of the parameters and not their physical origin.

Chapter 5

Herbertsmithite

introduction sur les liquides de spin

Computational Informations

The structure studied was taken from a X-ray study, the Hydrogen position were optimised using periodic DFT with PBE functional on the Quantum Espresso code.

Density functional theory calculations were performed on the ORCA package with def2-TZVP basis set on all atoms and the ωB97X-D3 functional which has shown to provide very good value of magnetic couplings. Wave-function base method were carried out on the MOLCAS program and CASDI codes with the extendend ANO-RCC basis set (6s5p3d2f for Cu and Zn, 4s3p2d for O, 4s3p1d for Cl and 2s1p for H)

The embedding's pseudopotential were set to the SDD Effective Core Potentiel (ECP) for ORCA calculations and *ab initio* model potentials (AIMP) of MOLCAS calculations. The quality of the embedding was checked by comparing the value of J_1 using the B3LYP functional for embedded cluster and periodic calculations (using the Crystal code). The J1 values are in perfect agreement: 240K for periodic and 239K for embedded cluster. As we will see below, these B3LYP values slightly overestimate the coupling but demonstrate the adequacy of the material model adopted in this study.

5.1 Density-Functional Theory study

In a first approximation, the isotropic behavior of Herbertsmithite is described by an unique first neighbor coupling. The highly-correlated nature of such system suggests the possibility of longer range interaction between copper ions seprated by one or more neighbor. To explore this possibility, the need to compute large fragments arises making the appplication of wave-function based method complicated. First the number of Cu^{2+} into the fragment has a direct impact on the size of the active space, even restricting to one orbital/ one electron per copper centrer lead to convergence troubles in the calculations. Also, the number of determinant and spin states generated forbid the use of Post-CASSCF method which are crucial for good estimation of magnetic couplings. Finally, the number of spin states render the analytical derivation complicated with

large matrices to diagonalize. As such, Density Functional Theory provides a good middle ground to compute large systems. It also presents some incoveniences, the DFT wavefunction is monodeterminantal and usually not an eigenfunction of the $\hat{S}^2$ operator which prevents the use of the HDVV Hamiltonian. Nevertheless, the combinated use of Broken-Symmetry DFT (BS-DFT) and the Ising Hamiltonian provides a good way to obtain an estimation of the couplings in the system. The Broken-Symmetry approach rely on the computation of DFT solutions where the M_S value of spin moment of each copper ion of the fragment have been imposed beforehand to $\pm\frac{1}{2}$. It is then possible to obtains multiple solutions per fragments to make a connection between the energy differences of each solutions and the Ising Hamiltonian. Additionaly, the time necessary for a DFT calculation and for the derivation of its analytical solution allows for the exploration of different properties of the embedding such as the size of the fragments and overall quality of it.

In-plane couplings

In a first description, a fragment presenting only the first neighbor coupling was introduced with three copper ions as shown on figure 5.1. Four solutions are possible to compute with $M_S \geq 0$, first a $M_S = 3/2$ where all magnetic moment of the Cu^{2+} ions are aligned creating a fully ferromagnetic solution. Then three other solutions are possible by switching the M_S value of one of the Cu^{2+} ion to $-1/2$. If the choice of fragment and construction of the embedding are done correctely, this should lead to three equal differences of energy as these solutions are treated equally by the Ising Hamiltonian.

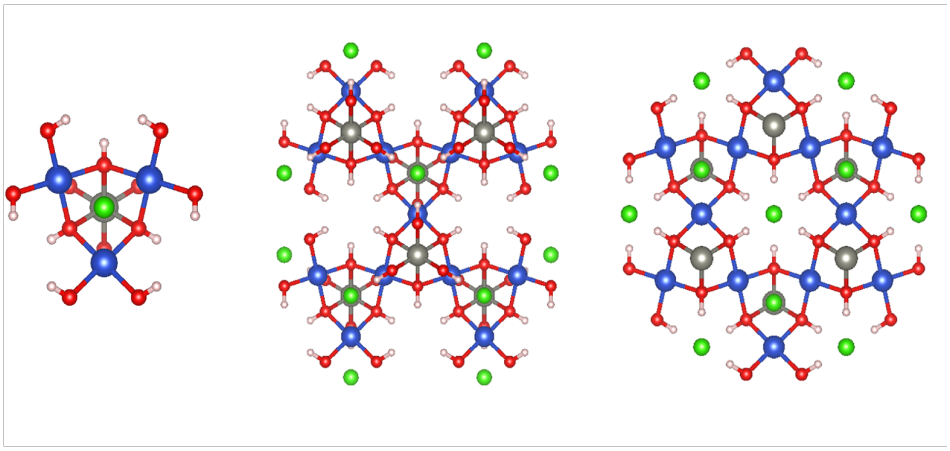

Figure 5.1: Fragments considred for DFT calculations for in plane component, (a) trimer (b) 13Cu (c)12Cu

Let us call the highest occupied orbital of each copper ion a,b and c. The Slater determinant describing the high spin solution (M_S=+1/2 on each Cu^{2+}) can then be written $|abc|$ while the low spin solutions (one of the M_S value is switched to $-1/2$) are written $|ab\overline{c}|$,$|a\overline{b}c|$ and $|\overline{a}bc|$. Applying $\hat{H}_{Ising} = \sum_{i,j} J_1 \hat{S}_{i,z}\hat{S}_{j,z}$ to the high spin (HS) solution $|abc|$ gives the eigenvalue $\frac{3}{2}J_1$ while the application on the low spin (LS)

solutions gives the eigenvalue $\frac{1}{2}J_1$. The Ising Hamiltonian has no effect on the spin variable of each centre, hence its matrix representation is diagonal:

H_{Ising}	$\|abc\|$	$\|ab\bar{c}\|$	$\|a\bar{b}c\|$	$\|\bar{a}bc\|$
$\|abc\|$	$\frac{3}{2}J_1$	0	0	0
$\|ab\bar{c}\|$	0	$\frac{1}{2}J_1$	0	0
$\|a\bar{b}c\|$	0	0	$\frac{1}{2}J_1$	0
$\|\bar{a}bc\|$	0	0	0	$\frac{1}{2}J_1$

The value of J_1 can then be extracted from the difference in energy between the high spin solution and low spin one:

$$J_1 = E_{HS} - E_{LS} \tag{5.1.1}$$

The same procedure of extraction can now be applied to larger fragment with the introduction of longer range couplings. The second fragment created included nine copper ions in total which allowed for the consideration of two new couplings, J_2 and J_3 represented on figure 5.2. It indicated that these couplings were small ($|J_2| \approx |J_3| \approx 1cm^{-1}$ each) with a large standard deviation. While these results provided good hindsight on the nature of these two couplings, the extraction was unsatisfactory. The source of this deviation is believed to be the environment of ions taking part in the interaction. These couplings involve ions at the border of the fragment whose neighboring atoms were not always explicitely computed compared to ions at the center of the fragment. As such, small convergence differences could alter the energy value obtained via DFT and cause such small deviation, . It was decided to increase the size of the fragment to twelve and thirteen copper ions (fragment (c) and (b) from figure 5.1) so that there would be ways account for these interaction within the center of the fragments.

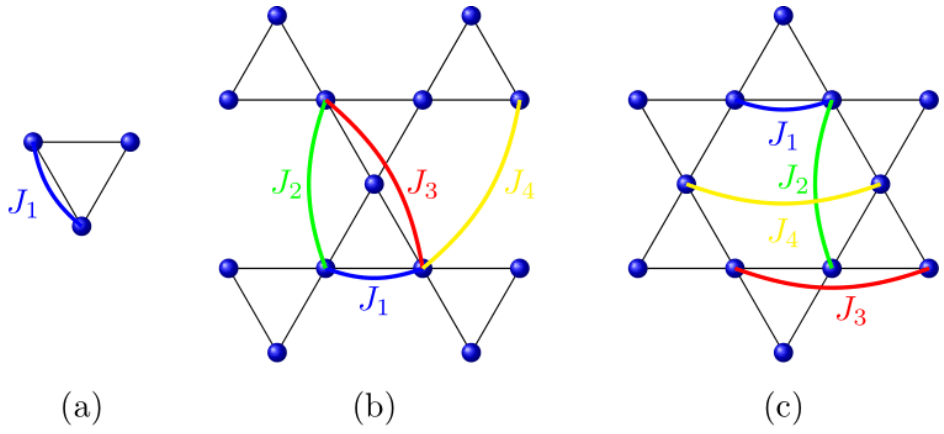

Figure 5.2: Schematic representation of the fragments and the couplings introduced

The results obtained for each couplings in the thre fragments are presented in table 5.1. The first thing to note is the good transferability with a small relative deviation from one cluster to the other. Note that with this convention of the Ising Hamiltonian

(a plus sign in front of the J term), a positive value indicates antiferromagnetism while negative indicates ferromagnetism. The closest neighbor interaction J_1 is in good agreement with values published in the litterature while J_2,J_3 and J_4 are very weak.

$J_i(K)$	(a)	(b)	(c)	d_{Cu-Cu} (Å)
J_1	178.0	191.2	181.0	3.42
J_2	-	0.5	0.4	5.91
J_3	-	-1.1	-1.0	6.83
J_4	-	-0.1	-0.2	6.83

These results highlight the mainly antiferromagnetic nature of these interactions with a leading interaction J_1 at least two order of magnitude higher than the other. This confirm the the use of models composed of only one J interaction, the negligenge of other couplings should cause no more than a small deviation.

Out-of-plane coupling

Another preoccupation of the model is the occupation disorder, cristallographic studies have identified two types of defects present at low-temperature. First the substitution of the Zn^{2+} inter-plane site with a Cu^{2+} ion, estimated with a 0.15 occurance rate, and second an Zn^{2+} entering the Kagome plane with a much smaller occurance rate ($<$0.05). In a similar approach, three clusters that were built to include the intersite ion are represented on figure 5.3a. Fragment (a) was designed to check the J_1 coupling, fragment (b) and (c) allow the exploration of both type of disorder.

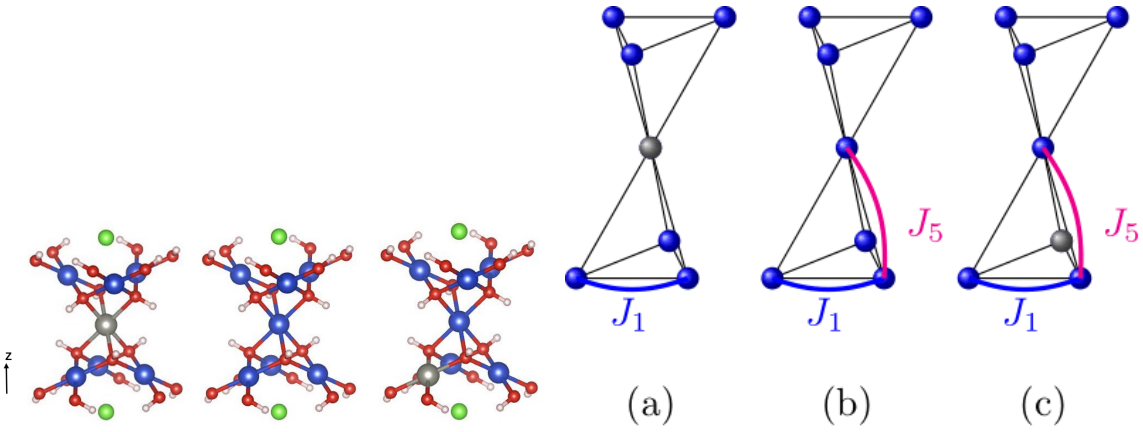

(a) *ab initio* (b) Couplings

Figure 5.3: Embedded clusters and associated model for intersite calculations

These fragments allows for the introduction of a new coupling J_5 between the intersite Cu^{2+} ion with an inplane one. Note that with a distance $d_{Cu-Cu} = 3.07$Å, it actually becomes the first neighbor coupling. Table 5.1 shows a J_1 coupling in accordance with previous calculation in all three clusters with now the presence of strong ferromagnetic coupling J_5. Its magnitude, $J_5 \approx -J_1/2$, could have a strong impact on the properties of this material and should in fact be taken into account in the model. Due to this

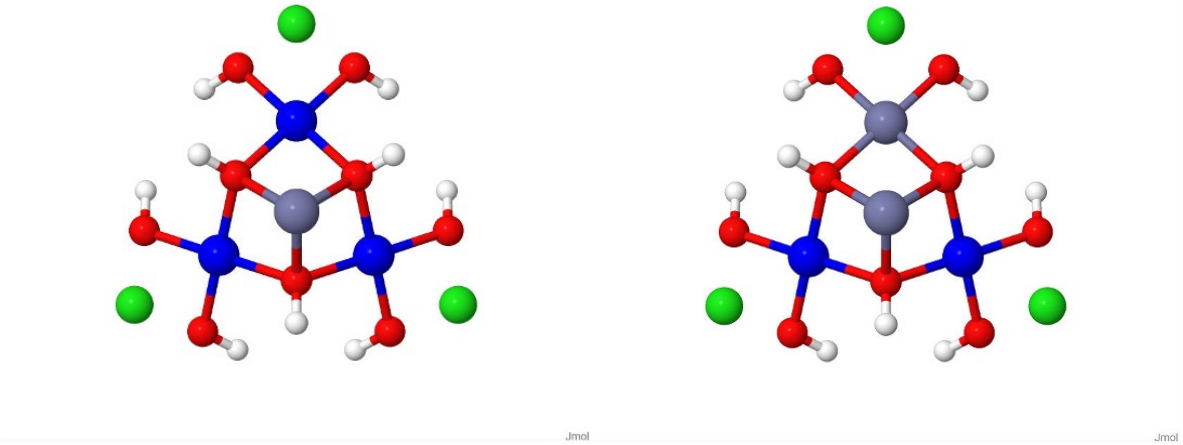

(a) Trimer (b) Dimer

Figure 5.4: Embedded clusters used for Wave-funciton computation

magnetic coupling, Herbertsmithtie might not be the perfect realisation of a Kagome-antiferromagnet and explain the difficulty to determine its nature as spin liquid.

$J_i(K)$	(a)	(b)	(c)
J_1	184.2	184.1	182.7
J_5	-	-83.4	-82.0

5.2 Wave-Function Theory study

A second purpose of this study was the determination of anisotropic interaction in the crystal. The extraction of such interactions follows the same procedure as described in chapter chapter 4. The computation of SO-states being very computationally demanding, this extraction will be resticted to two fragments of small size.

The first fragment, figure 5.4a, is similar to the one used for DFT calculation, with three copper ions arranged in an equilateral triangle. A second fragment 5.4b was designed by substituting one of the Cu^{2+} with a diamagnetic Zn^{2+}, both share rather close structural properties (charge, mass, ionic radius). As the d shell of the zinc ion is completely filled it will not take part in the magnetic interactions, leaving us with essentially a dimer to capture the interaction of only two Cu^{2+}. This approach has been studied in serveral other materials and we will see from the results that this substitution has little impact on the extracted values but can significally reduce ther overall study time.

5.2.1 Isotropic Coupling

To check the applicability of WFT calculation to this system, the first step was to try and reproduce the J_1 value. In both cluster, two type of active space were considered:

- one electron and orbital per magnetic center.
- all eletrons occupying the d shell of each magnetic center.

The first type of active space results in a CAS(2,2) for the dimer calculation which generates one triplet (S=1) and one singlet (S=0) state.

$$|1,1\rangle = |ab| \tag{5.2.1}$$

$$|1,0\rangle = \frac{1}{\sqrt{2}}(|a\bar{b}| - |b\bar{a}|) \tag{5.2.2}$$

$$|1,-1\rangle = |\bar{a}\bar{b}| \tag{5.2.3}$$

$$|0,0\rangle = \frac{1}{\sqrt{2}}(|a\bar{b}| + |b\bar{a}|) \tag{5.2.4}$$

The value of J_1 is then given by the difference in energy between the triplet and singlet state $J_1 = E(S=1) - E(S=0)$. The enlarged active space CAS(18,10) generates 25 Triplet and 25 Singlet states.

In the case of the trimer cluster, CAS(3,3) represents the minimum active space which generates 1 quartet (S=3/2) state and two doublet (S=1/2) states. The two doublet are degenerate if only one value of J is taken into account as is our case with an equilateral repartition of the copper ions.

$$|3/2,3/2\rangle = |abc| \tag{5.2.5}$$

$$|3/2,1/2\rangle = \frac{1}{\sqrt{3}}(|ab\bar{c}| + |a\bar{b}c| + |\bar{a}bc|) \tag{5.2.6}$$

$$|1/2,1/2\rangle_1 = \frac{1}{\sqrt{6}}(|ab\bar{c}| + |a\bar{b}c| - 2|\bar{a}bc|) \tag{5.2.7}$$

$$|1/2,1/2\rangle_2 = \frac{1}{\sqrt{2}}(|ab\bar{c}| - |a\bar{b}c|) \tag{5.2.8}$$

The expression of the m_s component with negative value were left out as they only differ by the number of up and down spins. The value of J_1 is then given by $J_1 = \frac{2}{3}(E(S=3/2) - E(S=1/2))$. The enlarges active space CAS(27,15) generates 125 Quartet and 250 Doublets states.

CASSCF calculation tends to "over"-localise the wavefunction on the metallic center, thus underestimating mechanism at the origing of the antiferromagnetic contribution to the J integral. As such it does not provides a good estimate but can nonetheless give informations about the nature of the coupling. Table 5.2.1 shows the results obtained at multiple level of calculation for different active space.

$J_1(K)$	CAS(2,2) CAS(3,3)	CAS(18,10) CAS(27,15)	CASPT2	DDCI1	DDCI3
Dimer	10.7	8.3	69.8	50.0	80.1
Trimer	8.2	7.7	56.0	50.7	60

These results indicate an antiferromagnetic J coupling with a large impact of dynamical correlation, yet these values do not match with the DFT calculations and the litterature.

An active space only composed of d-orbitals is not enough to achieve a correct estimation of the isotropic coupling in this system, to improve the description of the antiferromagnetic mechanisms it was then thought to bring the bridging ligand orbitals into the active space. The inclusion of the p-orbitals of the bridging oxygen presents a challenge, as they stay doubly occupied and do not contribute to the wave-function at CAS level, reaching a stable active space becomes challenging because of convergence issue. To avoid these troubles, a methodology based on the projection of the oxygen's p-orbitals onto the ligand's tail of the active orbitals was applied. This allows to obtain a reproducible active space with well defined orbitals represented on figure **??**.

It has been previously established that performing a DDCI1 calculation on a active space composed of the ligands orbitals in addition to the magnetic orbitals allows to obtain value of J coupling on par to a DDCI3 calculation. This allows to greatly reduce computational time, the active space is now composed of one electron/orbital per metallic center and two electrons in one orbital per oxygen (CAS(4,3) in the dinuclear and CAS(9,6) in the trinuclear fragment). This procedure has allowed the extraction of new values for J_1 in both fragment, $J_1 = 105.3cm^{-1}$ in the dinuclear cluster and $J_1 = 126.3cm^{-1}$ in the trinuclear cluster. Even if the dinuclear value of J_1 is lower, the coupling extracted from the trinuclear fragment is well within range of the expected value by both DFT and experiment.

5.2.2 Anisotropic interactions

The computation of the isotropic couplings was a way to assertain the validity of our methods and calibration of the embedded cluster method. The electronic structure of the compound seems to be well replicated with a satisfying extraction of the these coupling. The main purpose of this study can now be adressed, which is the extraction of anisotropic interactions. Theoretical model propose the inclusion of a weak Dzyaloshinskii-Moriya pseudo-vector along the out of plane direction to account for the behavior at low temperature but the symmetric tensor of anisotropy $\overline{\overline{D}}_{ij}$ is usually left out. Following the procedure explained in 4, all three components of the DMI were extracted as well as the D_{ij}-tensor.

Bi-nuclear calculation

Starting from the CASSCF wave-function with the enlarge active space of all 18 copper d-shell electrons and the 10 d-orbitals, computation of the SO-states was performed using the SO-RASSI method implemented in MOLCAS. The lowest part of the energy spectrum was corrected using the isotropic coupling value previously obtained. No assumption on the magnetic axes were made and so the extraction of all anisotropic parameters (9 in total) was performed using effective hamiltonian theory with a model space composed of the three M_S component of the triplet state and the singlet state. The matrix representation of the model Hamiltonian in the model space basis is:

H_{MS}	$\|1,-1\rangle$	$\|1,0\rangle$	$\|1,1\rangle$	$\|0,0\rangle$
$\langle 1,-1\|$	$\frac{J}{4}+\frac{D_{zz}}{4}$	$\frac{D_{xz}-iD_{yz}}{2\sqrt{2}}$	$\frac{(D_{xx}-D_{zz}-2iD_{xy})}{4}$	$\frac{d_y+id_x}{2\sqrt{2}}$
$\langle 1,0\|$	$\frac{D_{xz}+iD_{yz}}{2\sqrt{2}}$	$\frac{J}{4}-\frac{D_{zz}}{4}+\frac{(D_{xx}+D_{yy})}{4}$	$-\frac{D_{xz}-iD_{yz}}{2\sqrt{2}}$	$-\frac{id_z}{2}$
$\langle 1,1\|$	$\frac{(D_{xx}-D_{zz}+2iD_{xy})}{4}$	$-\frac{D_{xz}+iD_{yz}}{2\sqrt{2}}$	$\frac{J}{4}+\frac{D_{zz}}{4}$	$\frac{d_y-id_x}{2\sqrt{2}}$
$\langle 0,0\|$	$\frac{d_y-id_x}{2\sqrt{2}}$	$\frac{id_z}{2}$	$\frac{d_y+id_x}{2\sqrt{2}}$	$-\frac{3J}{4}-\frac{D_{zz}}{4}-\frac{(D_{xx}+D_{yy})}{4}$

The values obtained for both interaction expressed in Kelvin in the axis system of the cluster are:

$$\overline{\overline{D}}_{ij}\begin{pmatrix}1&0&0\\0&1&0\\0&0&1\end{pmatrix} \qquad \mathbf{d}_{ij}\begin{pmatrix}0\\4.73\\1.70\end{pmatrix}$$

The symmetric tensor can be diagonalized to extract the $D=-0.46K$ axial parameter and a small $E=0.13K$ rhombic term. These values are small and should have only little impact on the magnetic properties of this system however the DMI components are non negligible. The DMI value along the x-axis is naught, as expected from symmetry reason. Note that the in-plane component (along the y-axis) is larger than the out of plane component (along the z-axis), this result can be suprising but can be rationalized looking at the origins of the DMI component. It was demonstrated analyticaly that the DM-interaction comes from the hybdridization of the metal's d-orbitals. It showed that:

- a mixing between $d_{x^2-y^2}$ and d_{yz} or d_{xy} and d_{xz} generates a d_x component.
- a mixing between $d_{x^2-y^2}$ and d_{xz} or d_{xy} and d_{yz} generates a d_y component.
- a mixing between $d_{x^2-y^2}$ and d_{xy} or d_{xz} and d_{yz} generates a d_z component.

This mixing can be clearly observed on figure 5.5, and from the expression of one of these magnetic orbitals on the Cartesian d-orbitals of one copper ion : $0.4889d_{x^2-y^2}+0.2120d_{xz}-0.2841d_{xy}-0.3666d_{yz}$.

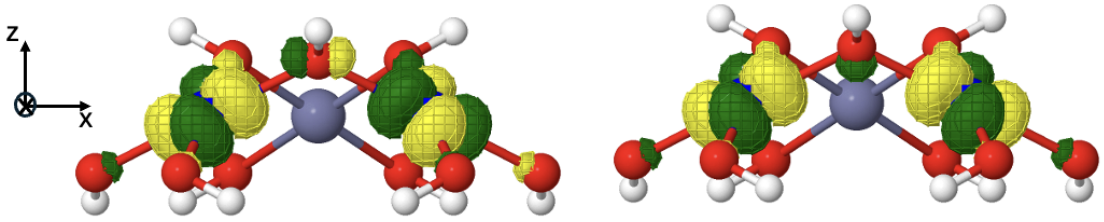

Figure 5.5: CAS(2,2)SCF magnetic orbitals calculated on the dimer fragment

Different configuration for the dimer cluster were explored to make sure the values extracted were not affected by which "couple" of Cu^{2+} ions were chosen. The extra

zinc ion was swapped around all three in plane site followed by the same procedure of extraction. The same out of plane $|d_\perp|$ value and the same projection in the xy plane ($|d_\parallel|$) were found in all three calculations.

Trinuclear calculations

The extraction was then performed on the tri-nuclear fragment with an active space of 27 electrons in 15 orbitals. In the case of three magnetic center, the model Hamiltonian is now written:

$$\begin{aligned}\hat{H}_{MS} =& J_{12}\hat{\mathbf{S}}_1\cdot\hat{\mathbf{S}}_2 + \hat{\mathbf{S}}_1\cdot\overline{\overline{D}}_{12}\cdot\hat{\mathbf{S}}_2 + \mathbf{d}_{12}\cdot(\hat{\mathbf{S}}_1\times\hat{\mathbf{S}}_2)\\ & J_{12}\hat{\mathbf{S}}_2\cdot\hat{\mathbf{S}}_3 + \hat{\mathbf{S}}_2\cdot\overline{\overline{D}}_{23}\cdot\hat{\mathbf{S}}_3 + \mathbf{d}_{23}\cdot(\hat{\mathbf{S}}_2\times\hat{\mathbf{S}}_3)\\ & J_{13}\hat{\mathbf{S}}_1\cdot\hat{\mathbf{S}}_3 + \hat{\mathbf{S}}_1\cdot\overline{\overline{D}}_{13}\cdot\hat{\mathbf{S}}_3 - \mathbf{d}_{13}\cdot(\hat{\mathbf{S}}_1\times\hat{\mathbf{S}}_3)\end{aligned} \tag{5.2.9}$$

Note the negative sing in front of the last term d_{13} which originates from the permutation realtionship specific to the DMI (d_{13}=-d_{31}). On the other hand we set $J_{12} = J_{23} = J_{13}$ and let the D_{ij}-tensor be expressed in the axis system of the cluster with 6 paramaters each. First, we can obtain the matrix representation of this Hamiltonian in the basis of the determinant formed from the three magnetic orbitals on each site (a, b and c) located on each copper center:

To express this matrix in the coupled basis, *i.e* in the basis formed from the m_s components of the quartet and two doublet states, one has to build the transofrmation matrix. This matrix can be obtained using the Clebsch-Gordan coefficients or by diagonalizing the HDvV Hamiltonian representation matrix and using the eigenvectors as the transition matrix.

U	$\lvert\frac{3}{2},\frac{3}{2}\rangle$	$\lvert\frac{3}{2},\frac{1}{2}\rangle$	$\lvert\frac{3}{2},-\frac{1}{2}\rangle$	$\lvert\frac{3}{2},\frac{3}{2}\rangle$	$\lvert\frac{1}{2},\frac{1}{2}\rangle_1$	$\lvert\frac{1}{2},-\frac{1}{2}\rangle_1$	$\lvert\frac{1}{2},\frac{1}{2}\rangle_2$	$\lvert\frac{1}{2},-\frac{1}{2}\rangle_2$
$\langle abc\rvert$	1	0	0	0	0	0	0	0
$\langle ab\bar{c}\rvert$	0	$\frac{1}{\sqrt{3}}$	0	0	0	0	$-\frac{2}{\sqrt{6}}$	0
$\langle a\bar{b}c\rvert$	0	$\frac{1}{\sqrt{3}}$	0	0	$-\frac{1}{\sqrt{2}}$	0	$\frac{1}{\sqrt{6}}$	0
$\langle \bar{a}bc\rvert$	0	$\frac{1}{\sqrt{3}}$	0	0	$\frac{1}{\sqrt{2}}$	0	$\frac{1}{\sqrt{6}}$	0
$\langle a\bar{b}\bar{c}\rvert$	0	0	$\frac{1}{\sqrt{3}}$	0	0	0	0	$-\frac{2}{\sqrt{6}}$
$\langle \bar{a}b\bar{c}\rvert$	0	0	$\frac{1}{\sqrt{3}}$	0	0	$-\frac{1}{\sqrt{2}}$	0	$\frac{1}{\sqrt{6}}$
$\langle \bar{a}\bar{b}c\rvert$	0	0	$\frac{1}{\sqrt{3}}$	0	0	$\frac{1}{\sqrt{2}}$	0	$\frac{1}{\sqrt{6}}$
$\langle \bar{a}\bar{b}\bar{c}\rvert$	0	0	0	1	0	0	0	0

U	$\left\vert\frac{3}{2},\frac{3}{2}\right\rangle$	$\left\vert\frac{3}{2},\frac{1}{2}\right\rangle$	$\left\vert\frac{3}{2},-\frac{1}{2}\right\rangle$	$\left\vert\frac{3}{2},\frac{3}{2}\right\rangle$	$\left\vert\frac{1}{2},\frac{1}{2}\right\rangle_1$	$\left\vert\frac{1}{2},-\frac{1}{2}\right\rangle_1$	$\left\vert\frac{1}{2},\frac{1}{2}\right\rangle_2$
$\left\langle\frac{3}{2},\frac{3}{2}\right\vert$	$\frac{3J}{4}$	0	0	0	$-\frac{\sqrt{2}i}{8}(\mathbf{e}_x+i\mathbf{e}_y)(2\mathbf{d}_{12}-\mathbf{d}_{13}-\mathbf{d}_{23})$	0	$\frac{\sqrt{6}i}{8}(\mathbf{e}_x+i\mathbf{e}_y)(\mathbf{d}_{13}-\mathbf{d}$
$\left\langle\frac{3}{2},\frac{1}{2}\right\vert$	0	$\frac{3J}{4}$	0	0	$-\frac{\sqrt{6}}{12}\mathbf{e}_z(2\mathbf{d}_{12}-\mathbf{d}_{13}-\mathbf{d}_{23})$	$-\frac{\sqrt{6}}{24}(\mathbf{e}_x+i\mathbf{e}_y)(2\mathbf{d}_{12}-\mathbf{d}_{13}-\mathbf{d}_{23})$	$\frac{\sqrt{2}i}{4}\mathbf{e}_z(\mathbf{d}_{13}-\mathbf{d}_{23})$
$\left\langle\frac{3}{2},\frac{-1}{2}\right\vert$	0	0	$\frac{3J}{4}$	0	$-\frac{\sqrt{6}}{24}(\mathbf{e}_x+i\mathbf{e}_y)(2\mathbf{d}_{12}-\mathbf{d}_{13}-\mathbf{d}_{23})$	$-\frac{\sqrt{6}}{12}\mathbf{e}_z(2\mathbf{d}_{12}-\mathbf{d}_{13}-\mathbf{d}_{23})$	$-\frac{\sqrt{2}i}{8}(\mathbf{e}_x+\mathbf{e}_y)(2\mathbf{d}_{12}-\mathbf{d}_{13}$
$\left\langle\frac{3}{2},\frac{-3}{2}\right\vert$	0	0	0	$\frac{3J}{4}$	0	0	0
$\left\langle\frac{1}{2},\frac{1}{2}\right\vert_1$	0	0	0	0	$-\frac{3J}{4}$	0	0
$\left\langle\frac{1}{2},\frac{-1}{2}\right\vert_1$	0	0	0	0	0	$-\frac{3J}{4}$	0
$\left\langle\frac{1}{2},\frac{1}{2}\right\vert_2$	0	0	0	0	0	0	$\frac{3J}{4}$
$\left\langle\frac{1}{2},\frac{-1}{2}\right\vert_2$	0	0	0	1	0	0	0

The symmetric tensor terms (6 each, 18 total) were left out for clarity Following the same procedure with an active space of 27 electrons in 15 orbitals